ELSEVIER

Journal of Fluids and Structures 23 (2007) 117–142

JOURNAL OF FLUIDS AND STRUCTURES

www.elsevier.com/locate/jfs

Submerged fluid-filled cylindrical shell subjected to a shock wave: Fluid–structure interaction effects

S. Iakovlev

Department of Engineering Mathematics, Dalhousie University, Halifax, Nova Scotia, Canada B3J 2X4

Received 21 December 2004; accepted 8 July 2006
Available online 11 October 2006

Abstract

A submerged fluid-filled circular cylindrical shell subjected to a shock wave propagating in the external fluid is considered. The study focuses on a number of acoustic and structural effects taking place during the interaction. Specifically, the influence of the acoustic phenomena in the fluid on the stress–strain state of the shell is analysed using two different visualization techniques. The effect that the parameters of the shell have on the internal acoustic field is addressed as well, and the 'shock transparency' of various shells is discussed. Special attention is paid to the analysis of the contribution of the terms in the shell equations representing bending stiffness, and the limits of applicability of the membrane theory of thin shells are discussed in the fluid–structure interaction context. The possibility of cavitation in the internal fluid is investigated, and the effect that cavitation could have on the structural dynamics of the shell is discussed. The present paper is a follow-up of the author's earlier study of the interaction between fluid-filled cylindrical shells and external shock waves.

1. Introduction

The interaction between fluid-contacting elastic shells and shock loads is a complex dynamic process in which the role of acoustic phenomena in the fluid(s) is as important as that of elastic phenomena in the structure. The coupling between these two groups of effects is what makes the interaction so interesting and challenging to study. However, it appears that over the years some aspects of the shell–shock interaction have received more attention than others. For example, stress–strain states of shock-loaded shells have been extensively studied for at least five decades [e.g., Mindlin and Bleich (1953), Geers (1969), Huang and Wang (1970), Huang (1979a,b), Andelfinger (1994), Wardlaw and Luton (2000)] as have been various fluid dynamics phenomena for shock waves impinging on rigid structures [e.g., Bryson and Gross (1961), Heilig (1969), Takayama (1987), Hermann et al. (1987), Ofengeim and Drikakis (1997), Heilig (1999), Oakley et al. (2001), Sun et al. (2003)]. At the same time, significantly fewer studies have been published on other fluid–structure interaction phenomena such as, for example, acoustic fields induced by elastic structures responding to shock waves or acoustic pulses [e.g., Merlen et al. (1995), Takano et al. (1997), Ahyi et al. (1998)]. It also appears that certain types of shell systems have attracted much more attention that others. Specifically, most of the mentioned works addressed the case of an external loading on an empty submerged elastic shell or rigid structure, perhaps owing to a strong and well-funded interest of the world's navies in submersible vehicles.

E-mail address: serguei.iakovlev@dal.ca.

0889-9746/$ - see front matter
doi:10.1016/j.jfluidstructs.2006.07.004

Nomenclature

c_f	sound speed in the fluid, $\hat{c}_f = 1$
c_s	sound speed in the shell material, $\hat{c}_s = c_s c_f^{-1}$
I_n	modified Bessel function of the first kind of order n
h_0	thickness of the shell, $\hat{h}_0 = h_0 r_0^{-1}$
p_0	incident pressure, $\hat{p}_0 = p_0 \rho_f^{-1} c_f^{-2}$
p_α	peak incident pressure, $\hat{p}_\alpha = p_\alpha \rho_f^{-1} c_f^{-2}$
p_r^i	internal radiation pressure, $\hat{p}_r^i = p_r^i \rho_f^{-1} c_f^{-2}$
p_s	total pressure acting on the shell surface, $\hat{p}_s = p_s \rho_f^{-1} c_f^{-2}$
r	radial coordinate of the polar coordinate system, $r = \varrho r_0^{-1}$
r_0	radius of the shell, $\hat{r}_0 = 1$
R_0	radial distance to the source of the incident wave, $\hat{R}_0 = R_0 r_0^{-1}$
S_R	incident shock wave stand-off, $\hat{S}_R = S_R r_0^{-1}$
t	time, $t = \tau c_f r_0^{-1}$
v^*	transverse displacement of the middle surface of the shell, $v = v^* r_0^{-1}$
w^*	normal displacement of the middle surface of the shell, $w = w^* r_0^{-1}$
δ	dimensionless mass per unit area of the shell
θ	angular coordinate of the polar coordinate system
λ	exponential decay rate, $\hat{\lambda} = \lambda c_f r_0^{-1}$
ν	Poisson's ratio
ξ_n^i	response functions of the problem, internal fluid
ρ_f	density of the fluid, $\rho_f = 1$
ρ_s	density of the shell material, $\hat{\rho}_s = \rho_s \rho_f^{-1}$
ϱ	radial coordinate of the polar coordinate system, $r = \varrho r_0^{-1}$
τ	time, $t = \tau c_f r_0^{-1}$
ϕ	fluid velocity potential, $\hat{\phi} = \phi c_f^{-1} r_0^{-1}$
ϕ_0	fluid velocity potential in the incident wave, $\hat{\phi}_0 = \phi_0 c_f^{-1} r_0^{-1}$
ϕ_d	fluid velocity potential in the diffracted wave, $\hat{\phi}_d = \phi_d c_f^{-1} r_0^{-1}$
ϕ_r^e	fluid velocity potential in the external radiated wave, $\hat{\phi}_r^e = \phi_r^e c_f^{-1} r_0^{-1}$
ϕ_r^i	fluid velocity potential in the internal radiated wave, $\hat{\phi}_r^i = \phi_r^i c_f^{-1} r_0^{-1}$

Other symbols are defined in the text.

In contrast, some shell set-ups do not seem to have generated much interest in the fluid–structure interaction research community. For example, acoustic fields formed *inside* fluid-filled submerged shells experiencing *external* shock loads appear to have received very little attention. Even though such a system is less common than its evacuated counterpart, there still are a number of important industrial applications that can be successfully modelled using such a set-up. An underwater oil pipeline is probably the most apparent example, with cooling systems and offshore liquid storage tanks being other systems which can be analysed using the 'filled shell' model. The environmental impact associated with accidents involving, for example, oil pipelines, can be truly detrimental, and designing safer and more shock-resistant structures has always been one of the industry's top priorities. Along with the practical demand, the complexity of shell–shock interaction has always been of theoretical interest as well. Therefore, detailed study of the interaction between a submerged fluid-filled cylindrical shell and an external shock wave definitely appears to be of interest.

Such a study has recently been initiated by the author (Iakovlev, 2006), and a number of phenomena occurring in the system were considered, such as the dynamics of the internal pressure field and radiation into the fluid of elastic waves propagating in the shell. However, some effects that are of both theoretical and practical interest were left out of that study, so the complete picture of the interaction has not yet been rendered. The goal of the present paper is to continue the work initiated earlier and to deliver a more in-depth analysis of the interaction.

2. Mathematical model

We consider a circular cylindrical shell of radius r_0 and thickness h_0, and assume that $h_0/r_0 \ll 1$. We also assume that the deflections of the shell surface are small compared to its thickness, and therefore linear theory of shells can be applied. The transverse and normal middle surface displacements are v^* and w^*, respectively. The shell material is characterized by density ρ_s, sound speed c_s, and Poisson's ratio ν. The shell is submerged into and filled with linearly compressible, irrotational, nonviscous fluid of density ρ_f. The sound speed in the fluid is c_f. The shell is subjected to a cylindrical shock wave with the source located at the distance R_0 from the axis of the shell. Polar coordinates (ϱ, θ) based on the axis of the shell are employed. The schematic of the problem is shown in Fig. 1.

The fluids are governed by the wave equation

$$\nabla^2 \phi = \frac{1}{c_f^2} \frac{\partial^2 \phi}{\partial \tau^2}, \tag{1}$$

where ϕ is the fluid velocity potential, and τ is time.

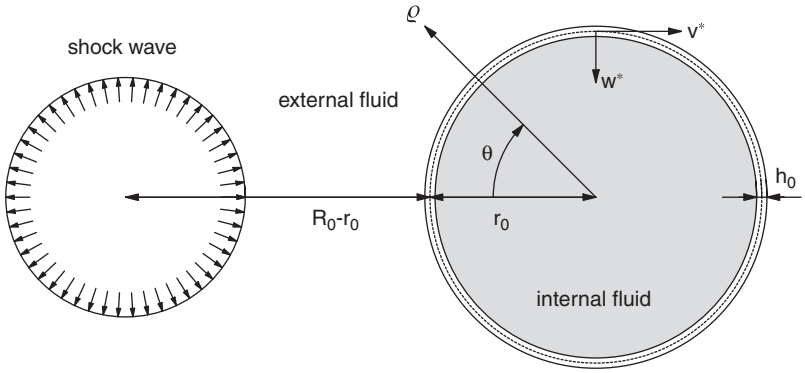

Fig. 1. Schematic of the problem.

If we assume the Love–Kirchhoff hypothesis, the shell equations in displacements are [their detailed derivation using Hamilton's principle can be found in, e.g., Junger and Feit (1972)]

$$\frac{1}{r_0^2}\frac{\partial^2 v^*}{\partial\theta^2}-\frac{1}{r_0^2}\frac{\partial w^*}{\partial\theta}+k_0^2\left(\frac{1}{r_0^2}\frac{\partial^3 w^*}{\partial\theta^3}+\frac{1}{r_0^2}\frac{\partial^2 v^*}{\partial\theta^2}\right)=\frac{1}{c_s^2}\frac{\partial^2 v^*}{\partial\tau^2}, \tag{2}$$

$$\frac{1}{r_0^2}w^*-\frac{1}{r_0^2}\frac{\partial v^*}{\partial\theta}+k_0^2\left(\frac{1}{r_0^2}\frac{\partial^4 w^*}{\partial\theta^4}+\frac{1}{r_0^2}\frac{\partial^3 v^*}{\partial\theta^3}\right)=\chi p_s-\frac{1}{c_s^2}\frac{\partial^2 w^*}{\partial\tau^2}, \tag{3}$$

where $k_0^2=h_0^2/(12r_0^2)$, $\chi=(h_0\rho_s c_s^2)^{-1}$, and p_s is the pressure acting upon the shell surface. The surface pressure comprises several components, namely the incident pressure, diffraction pressure, external radiation pressure, and internal radiation pressure; the same applies to the fluid velocity potential. In the present work, we are mostly interested in the internal radiation pressure.

The problem formulation also includes a set of boundary conditions, namely the 'no-flow' condition on the interface

$$\left.\frac{\partial\phi_d}{\partial\varrho}\right|_{\varrho=r_0}=-\left.\frac{\partial\phi_0}{\partial\varrho}\right|_{\varrho=r_0}, \tag{4}$$

where ϕ_0 is the fluid velocity potential in the incident wave and ϕ_d is that in the diffracted wave, dynamic conditions for the internal and external radiated potentials, ϕ_r^i and ϕ_r^e, respectively,

$$\left.\frac{\partial\phi_r^i}{\partial\varrho}\right|_{\varrho=r_0}=-\frac{\partial w^*}{\partial\tau}, \tag{5}$$

$$\left.\frac{\partial\phi_r^e}{\partial\varrho}\right|_{\varrho=r_0}=-\frac{\partial w^*}{\partial\tau}, \tag{6}$$

conditions at infinity

$$\phi_d\longrightarrow 0 \quad\text{and}\quad \phi_r^e\longrightarrow 0 \quad\text{when}\quad \varrho\to\infty \tag{7}$$

and on the axis of the shell

$$-\infty<\phi_r^i|_{\varrho=0}<\infty, \tag{8}$$

the periodicity conditions θ-wise, and zero initial conditions.

To make the analysis more efficient (e.g., to avoid dealing with small numerical values of the time τ), we introduce a dimensionless formulation of the problem, normalizing all the variables to r_0, c_f, and ρ_f. Dimensionless time t, for example, is given by $t=\tau c_f r_0^{-1}$, and $t=2$ corresponds to the time it takes for the incident shock wave to move over the shell. With some exceptions, a hat over a dimensionless variable distinguishes it from its dimensional counterpart. In order to ensure a better applicability of the results, acoustic pressure fields are analysed in a dimensional form.

The acoustic part of the problem (i.e. the three boundary-value problems for the components of the fluid velocity potential) was approached using a rather standard methodology based on combining separation of variables with the Laplace transform technique. Then, a finite-difference solution of the modal form of the shell equations was coupled with the analytical solution of the acoustic part to compute the shell displacements and, eventually, simulate the internal

pressure field. As a result, the dimensionless internal radiation pressure $\hat{p}_r^i$ was obtained in the form of a Fourier series with time-dependent coefficients which, in turn, were expressed in terms of convolution integrals of the harmonics of the normal displacement of the shell surface with the response functions for the geometry considered, $\xi_n^i(r,t)$,

$$\hat{p}_r^i(r,\theta,t) = \sum_{n=0}^{\infty}\left\{\int_0^t \frac{\mathrm{d}^2 w_n(\eta)}{\mathrm{d}\eta^2}\,\xi_n^i(r,t-\eta)\,\mathrm{d}\eta\right\}\cos n\theta, \tag{9}$$

where

$$w(\theta,t) = \sum_{n=0}^{\infty} w_n(t)\cos n\theta, \tag{10}$$

and the Laplace transforms of $\xi_n^i(r,t)$, $\Xi_n^i(r,s)$, are given by

$$\Xi_n^i(r,s) = \frac{\mathrm{I}_n(rs)}{s\mathrm{I}_n'(s)}, \tag{11}$$

where I_n is the modified Bessel function of the first kind of order n. The details can be found in Iakovlev (2006).

3. Phenomena considered

In this paper, we focus on a number of phenomena that appear to be of interest in the shell–shock interaction context but which were not addressed in the companion paper (Iakovlev, 2006). We start with the analysis of the influence that the internal fluid has on the shell dynamics, and consider the stress–strain state of a submerged shell with and without internal fluid. This aspect of the interaction has been studied earlier [e.g., Iakovlev (2002)], but it is certainly of interest to look at it again now, when the images of the corresponding acoustic field are available. Then, we address a somewhat inverse problem, and analyse the influence that the shell has on the internal pressure field. Of particular interest here is to find out how various shell materials and thicknesses affect the geometry and amplitude of the acoustic waves propagating inside the shell. Next, we consider the distribution of the pressure on the shell surface. Even though the surface pressure acting upon shock-interacting shells is quite well-studied, it appears of interest to put it into the fluid–structure interaction perspective, i.e. to link it to a variety of elastic phenomena in the shell and acoustic effects in the fluid. Then, we focus on the analysis of the contribution of the terms representing bending stiffness in the shell equations. Even though this is not a physical phenomenon as such, establishing the limits of applicability of the membrane theory of shells to the problems of the class considered is definitely of interest. Finally, we discuss such an important aspect of shell–shock interaction as cavitation.

We consider a steel shell with $\rho_s = 7800\,\mathrm{kg/m^3}$ and $c_s = 5000\,\mathrm{m/s}$. Unless stated otherwise, the thickness-to-radius ratio is assumed to be $h_0/r_0 = 0.01$, with $r_0 = 1\,\mathrm{m}$ and $h_0 = 0.01\,\mathrm{m}$. The shell is submerged into and filled with water, $\rho_f = 1000\,\mathrm{kg/m^3}$ and $c_f = 1400\,\mathrm{m/s}$.

We continue to use the terminology introduced in the companion paper (Iakovlev, 2006), i.e. we refer to the points $\theta = 0$ and $\theta = \pi$ as the 'head point' and 'tail point', respectively. Furthermore, we call the pressure wave propagating in the internal fluid the 'internal shock wave' due to the fact that the pressure rise associated with this wave is very sharp, even though there is no pressure discontinuity. We also consider three different stages of the interaction which we term the 'downstream propagation' ($t = 0.00-2.00$), 'primary reflection and focusing' ($t = 2.00-3.00$), and 'upstream propagation and secondary reflection and focusing' ($t = 3.00-5.00$).

As for the incident wave, we only consider a shock wave with a large source stand-off (the distance between the shell and wave source). Namely, we assume the stand-off to be equal to four radii of the shell, $S_R = 4r_0$. This is due to the fact that the linear model employed provides most realistic results for shock waves with large stand-offs; for smaller stand-offs, much more sophisticated models are required to simulate the interaction acceptably accurately. The other two parameters of the incident wave, namely the peak pressure in the front and the exponential decay constant, are assumed to be $p_\alpha = 250\,\mathrm{kPa}$ and $\lambda = 0.0001314\,\mathrm{s}$, respectively.

4. Dynamics of the internal acoustic field

Analysis of the phenomena mentioned is much more efficient when a sequence of pressure snapshots illustrating the dynamics of the internal fluid is available. Even though such images can be found in the companion paper, the author felt that reproducing them here in colour is appropriate. Not only having all the snapshots in one place makes their use

more convenient, colour images also reveal some features that were not necessarily apparent from the halftone images found in Iakovlev (2006).

Fig. 2 shows the series of colour pressure snapshots for a steel shell with the thickness-to-radius ratio of 0.01, the 'default' case analysed most extensively in this study. Since the main purpose here is to have an informative visual representation of the dynamics of the process, the pressure magnitudes are not particularly important. For that reason, colours are assigned individually for each snapshot, with blues corresponding to the lowest pressure at that particular instant, the reds corresponding to the highest pressure, and the greens corresponding to the zero pressure. The instants at which the snapshots are taken do not follow any particular pattern and are chosen to ensure that the most important features of the interaction are well represented. The detailed discussion of the many acoustic phenomena observed can be found in the companion paper, and we do not repeat it here.

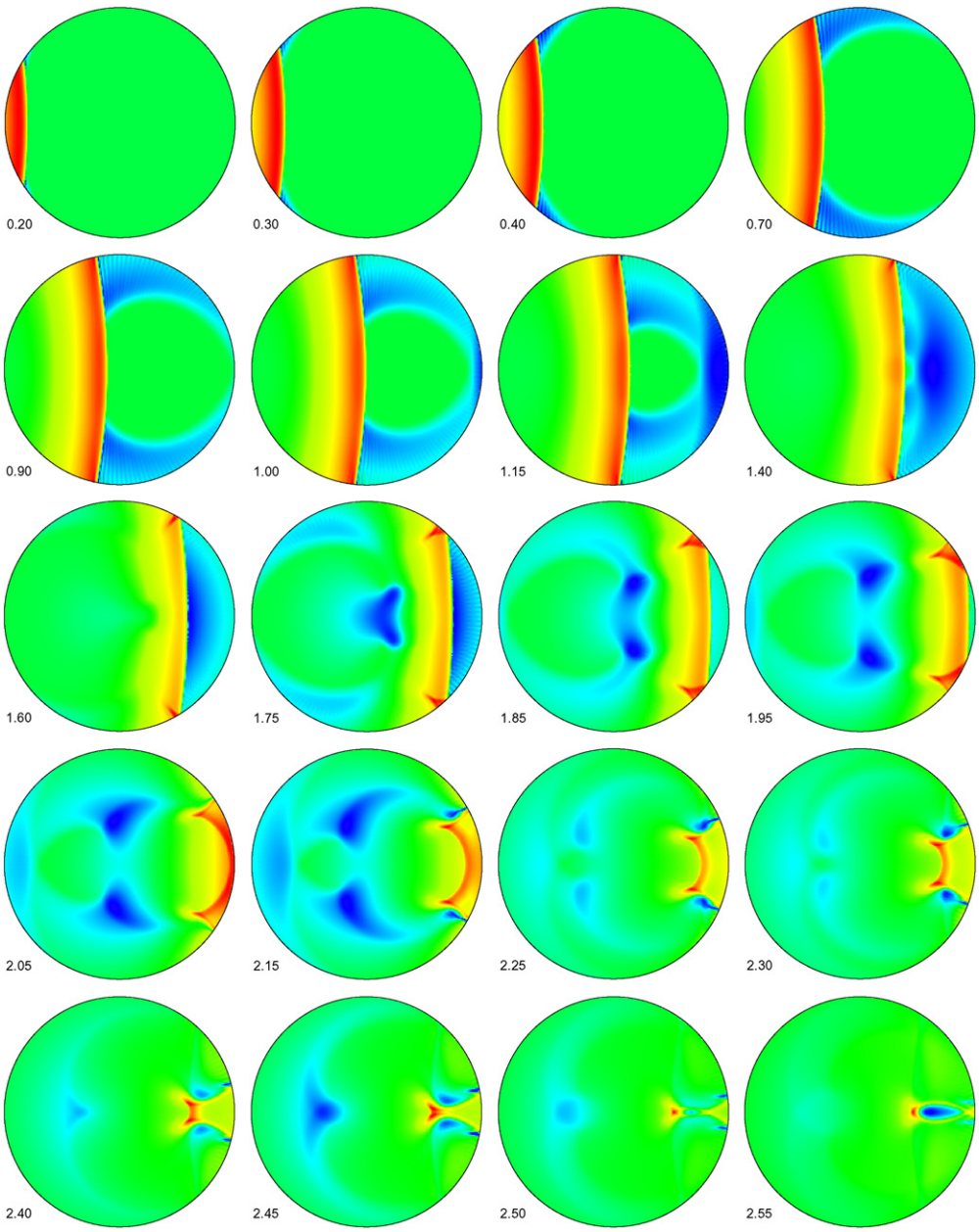

Fig. 2. Dynamics of the internal acoustic field: $t = 0.00-2.55$, and $t = 2.60-5.00$.

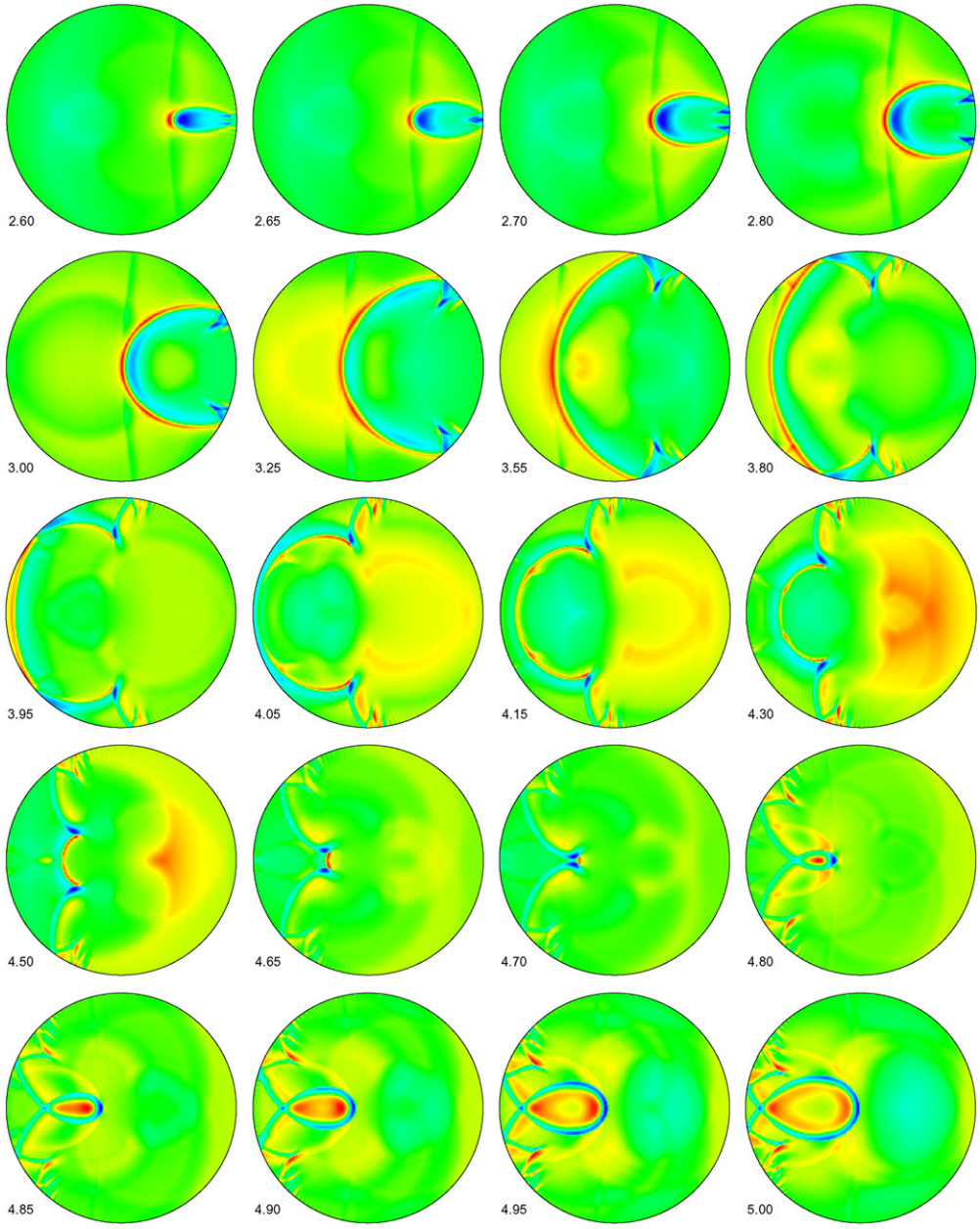

Fig. 2. (*Continued*)

5. Influence of the internal fluid on shell dynamics

It was demonstrated (Iakovlev, 2006) that the physics of the interaction between a shock wave and an elastic circular cylindrical shell is considerably more complex than that of the interaction between the same shock wave and a rigid-wall circular reflector. However, it was also established that in terms of the magnitude of the radiated pressure, the influence of the shell's elasticity on the dynamics of the internal fluid is mostly limited to a number of second-order effects (a scenario when cavitation develops is the only exception and is discussed later on). In view of that, it appears of interest to find out how significant the effect of the internal fluid on the dynamics of the shell is.

Figs. 3 and 4 show the strains in the middle surfaces of two identical (steel, $h_0/r_0 = 0.01$) submerged shells, one is fluid-filled and the other is empty. The actual strains were scaled in each case so that the maximum displayed strain

during the first circumnavigation is equal to approximately 20% of the shell radius; the actual strains in the fluid-filled shell are significantly lower than those in the empty one.

One can see that at the beginning of the interaction the strains are qualitatively identical in both cases. However, in the fluid-filled case, reflection of the internal shock wave from the tail region induces high-magnitude positive pressure. That, in turn, leads to large positive strains which are not present in the empty shell case. In other words, during the mid-interaction the stress–strain state of the empty shell is completely determined by elastic phenomena in the shell, whereas that of a fluid-filled shell is mostly governed by acoustic effects in the internal fluid. One therefore observes *qualitative* differences between the stress–strain states of a fluid-filled and empty shells subjected to the same shock wave [a fact that was established for the three-dimensional case in Iakovlev (2002)].

Fig. 5 shows the strains in the corresponding three-dimensional case, i.e. the same fluid-filled shell subjected to a spherical shock wave with the same peak incident pressure and exponential decay rate. The strains are scaled in the same way as in the previous plots. As one can see, the strain dynamics is qualitatively very similar in the two- and three-dimensional cases, the fact we referred to in the beginning of this study (Iakovlev, 2006) when discussing the appropriateness of the two-dimensional results for qualitative analysis of the three-dimensional interaction. Note that in the three-dimensional case, the strains decay faster than in the two-dimensional one (e.g., compare the snapshots at

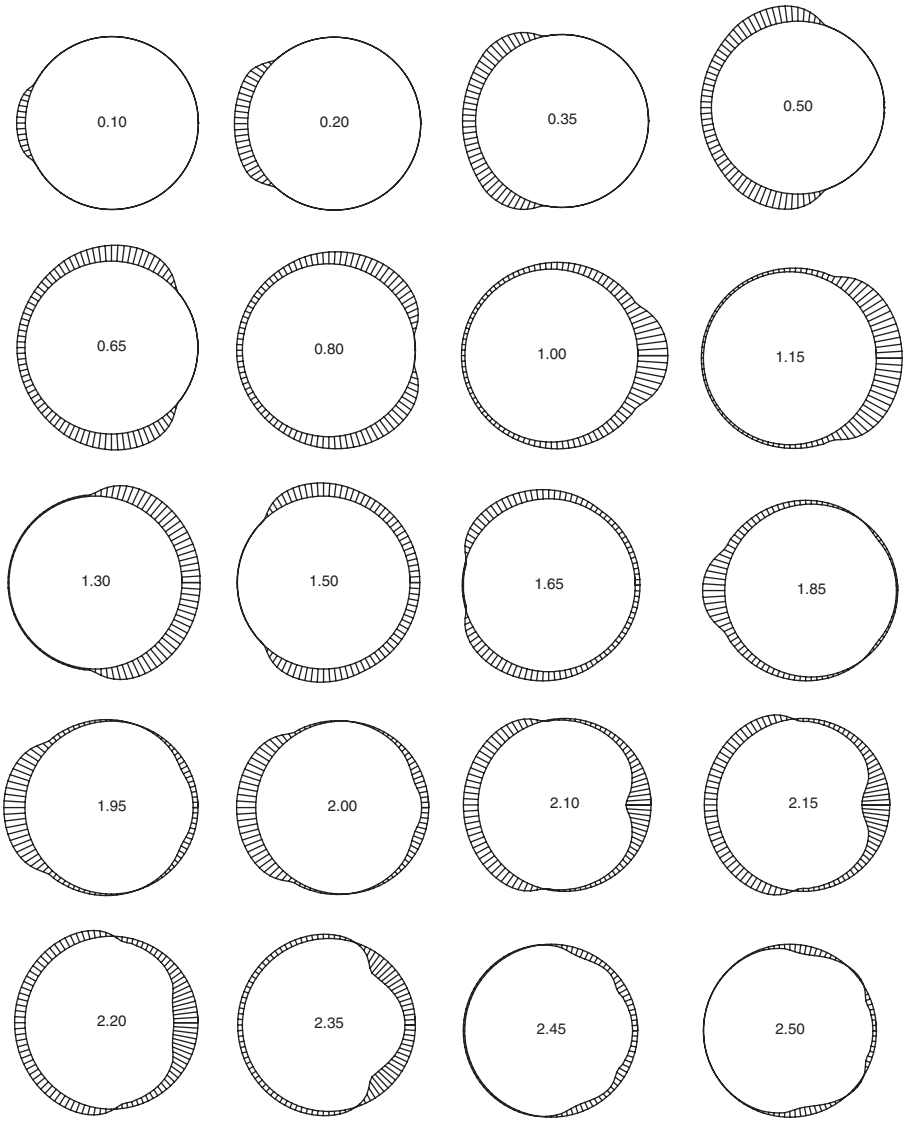

Fig. 3. Dynamics of the middle surface strain, the submerged fluid-filled shell.

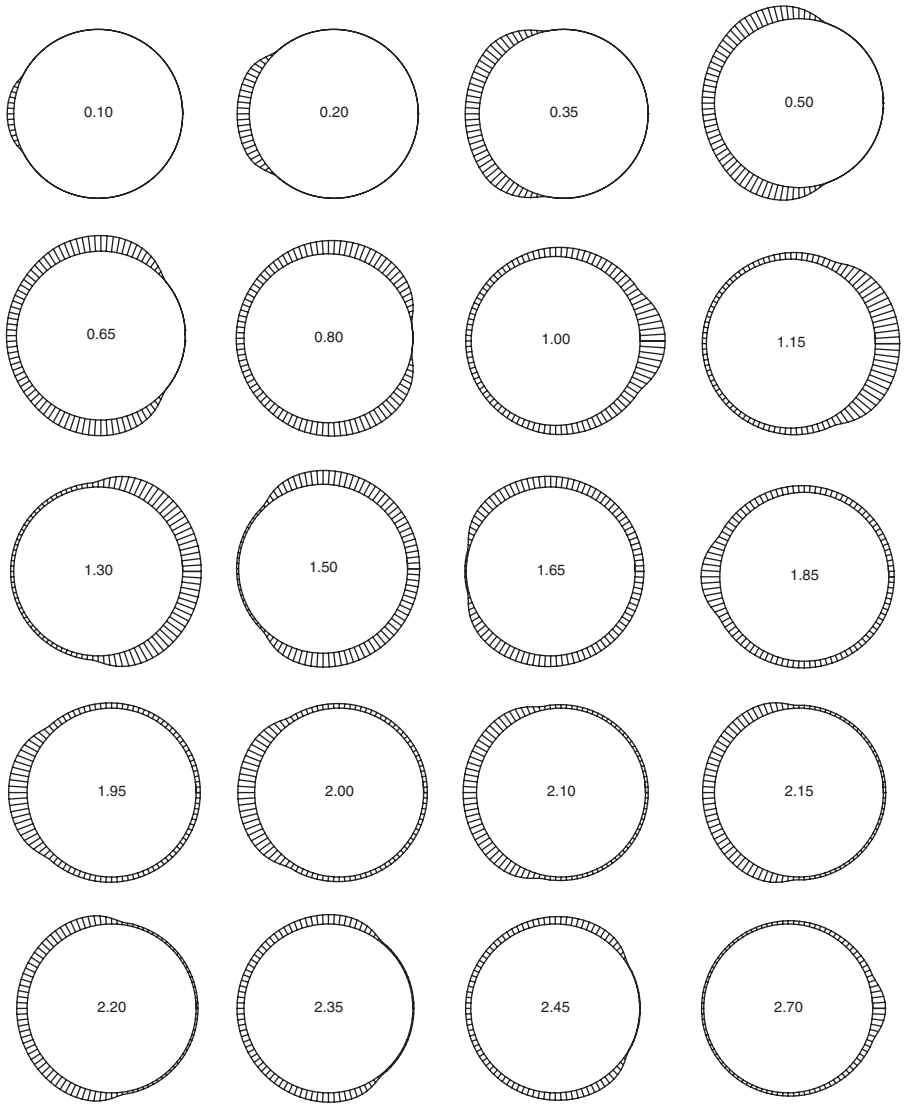

Fig. 4. Dynamics of the middle surface strain, the submerged empty shell.

$t = 1.85-2.00$). This is expected since in the three-dimensional case energy dissipation occurs in both the longitudinal and transverse directions whereas in the two-dimensional case the elastic waves propagate without longitudinal dissipation which results in much higher strains. One can also notice that in the three-dimensional case the strains induced by the internal shock wave reflecting from the tail region are lower than those in the two-dimensional case. This is not surprising either because of the faster dissipation of energy in the three-dimensional volume than in the (effectively) two-dimensional one.

It is interesting to point out that during the early downstream propagation, the strain waves originated when the incident wave first impinged on the shell do not seem to be significantly affected by either the internal or external shock waves directly, i.e. there is no noticeable strain change corresponding to the interaction between the shell and either wave. The normal displacements of the shell surface, in contrast, respond to the internal and external shock waves directly, and the position of the corresponding wavefronts can be easily identified from the sequential plots of the displacement dynamics, Fig. 6. The displacements shown are significantly enhanced (the maximum displacement is shown to be approximately 30% of the shell radius). The actual displacements are much smaller than the shell thickness.

Comparison of Fig. 6 with Fig. 7 which shows normal displacements for the corresponding submerged empty shell provides yet another perspective on the difference that the presence of the internal fluid makes in terms of the stress–strain state of the shell. Namely, one can see that for the empty shell, at $t = 1.0-2.0$ the amount by which the

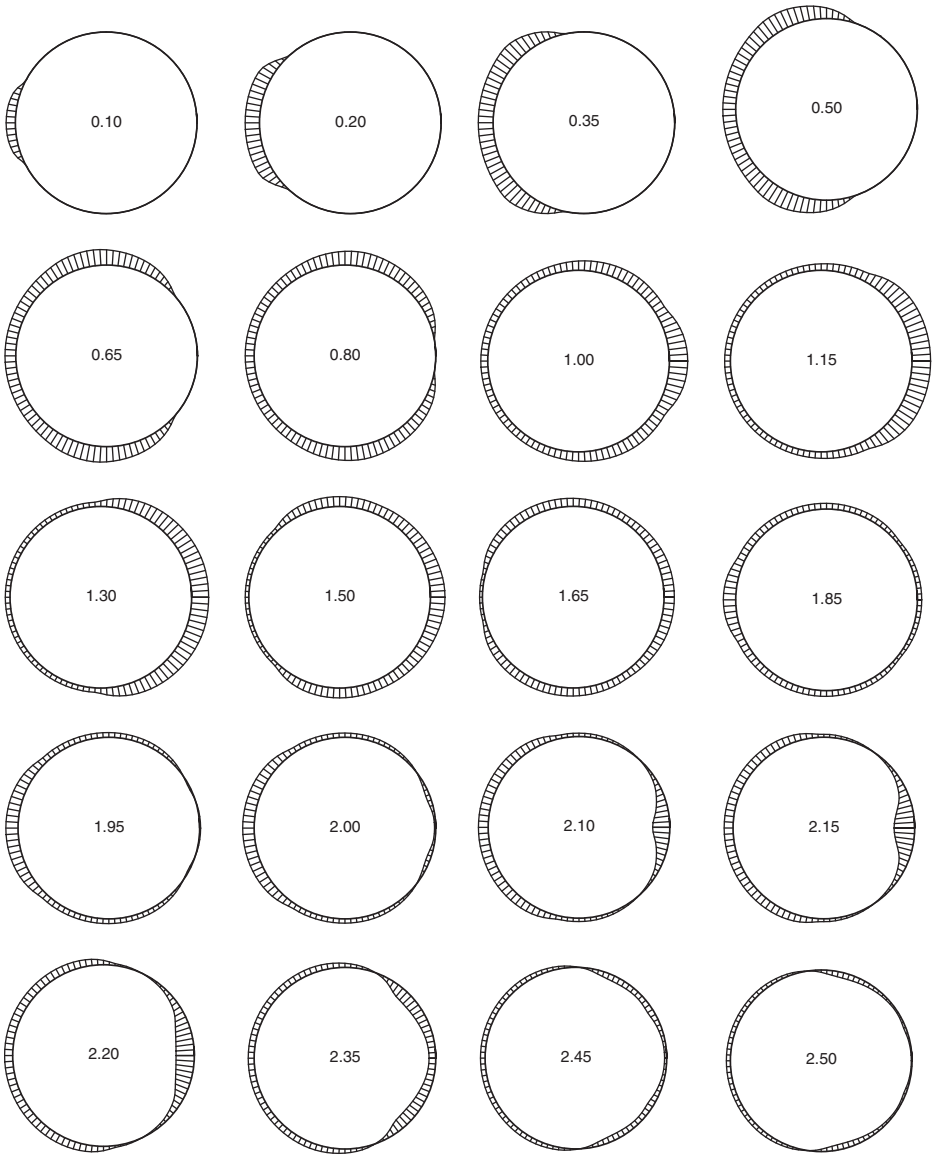

Fig. 5. Dynamics of the middle surface strain, the submerged fluid-filled shell—the three-dimensional case.

normal displacement increases is practically the same everywhere in the shadow region at any given instant, and there are no noticeable local irregularities in the distribution of w. In the fluid-filled case, however, the distribution of the normal displacement in the shadow region is very irregular, and the pressure rise corresponding to the internal shock wave is clearly detectable at the times in question. Furthermore, in the fluid-filled case, the displacement in the tail region starts to increase intensively at $t>2$ which indicates the response of the shell to the reflection of the internal shock wave from its surface.

Summarizing the observations outlined, we conclude that the influence of the internal fluid on the shell dynamics is much more significant than vice versa. Also, strains and displacements appear to have different dynamic features, and analysis of all the components of the stress–strain state is recommended to compose the most complete picture of the shell dynamics.

6. 'Shock transparency' of the shell

Discussing the shell–shock interaction, there is another practically important issue to address. Namely, since the existence of the internal shock wave is entirely due to the motion of the shell surface induced by the incident wave, it is

Fig. 6. Dynamics of the normal displacement, the submerged fluid-filled shell.

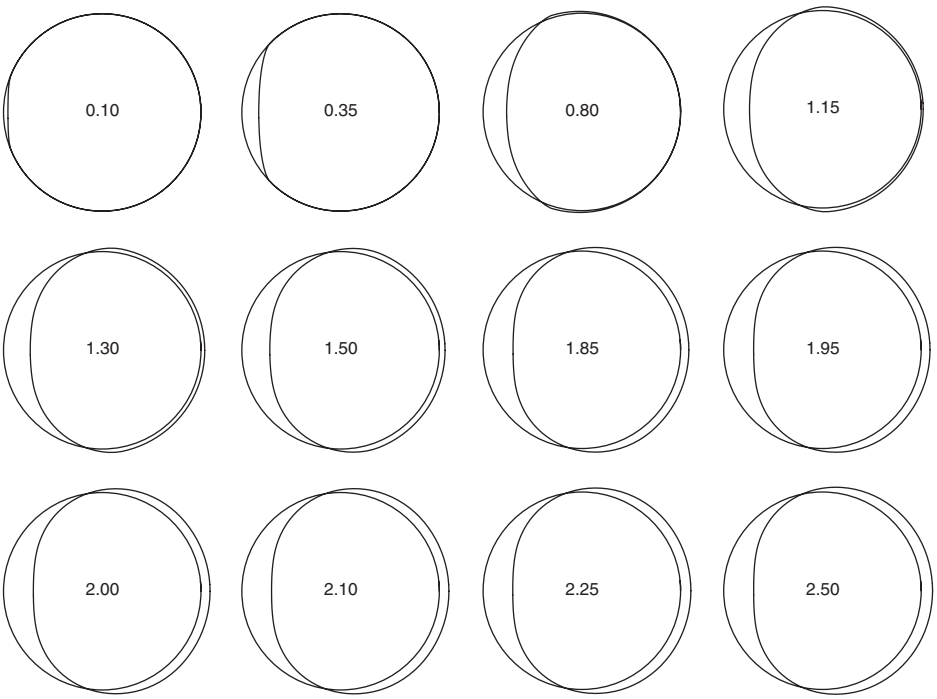

Fig. 7. Dynamics of the normal displacement, the submerged empty shell.

appropriate to talk about the 'transparency' of the shell to an incident shock wave. This notion of transparency is not new, and was discussed in the structural context by Huang (1979a, b) for concentric spherical and coaxial cylindrical shells, respectively. From the engineering point of view, understanding of 'shock transparency' of shells is quite important, and is particularly critical for two- and multi-shell structures such as double-hull submarines and advanced shock-resistant shell structures.

There are two questions to be answered here. First, how much is the internal shock wave influenced by the shell's geometrical and physical parameters, such as thickness, density, sound speed, and Poisson's ratio? Second, how much geometrically and physically different are the internal shock wave and the incident wave propagating in the same fluid in the absence of the shell? We emphasize that the notion of 'shock transparency' only makes sense in the beginning of the interaction, before acoustic effects due to the interaction of the internal shock wave and the shell become significant.

We start with the analysis of the acoustic fields inside shells of three different thicknesses. Fig. 8(b)–(d), shows the internal fields at $t = 0.70$ in the shells with the thickness-to-radius ratio of 0.005, 0.01, and 0.02, respectively; other parameters of the system are the same as before. To facilitate the comparison, the incident wave is shown in the external fluid. It should be emphasized that since neither the diffracted nor radiated waves are displayed, the shown external pressure distribution is *not* the actual external acoustic field. Fig. 8(a) shows the incident shock wave propagating in the fluid in the absence of the shell (the latter is still shown for reference purposes).

One can see that, as the thickness increases, the 'shock transparency' of the shell decreases, i.e. the maximum pressure in the internal shock wave becomes lower and lower. Even though this result is rather obvious, Fig. 8 helps one to quantify the pressure change. We also note that Fig. 8 provides yet another demonstration of the fact that the internal shock wave does not have a pressure discontinuity associated with it, whereas the incident one does. We also note that, since the materials of all three shells are the same, only the pressure magnitudes are different, not the geometries of the shell-induced fields.

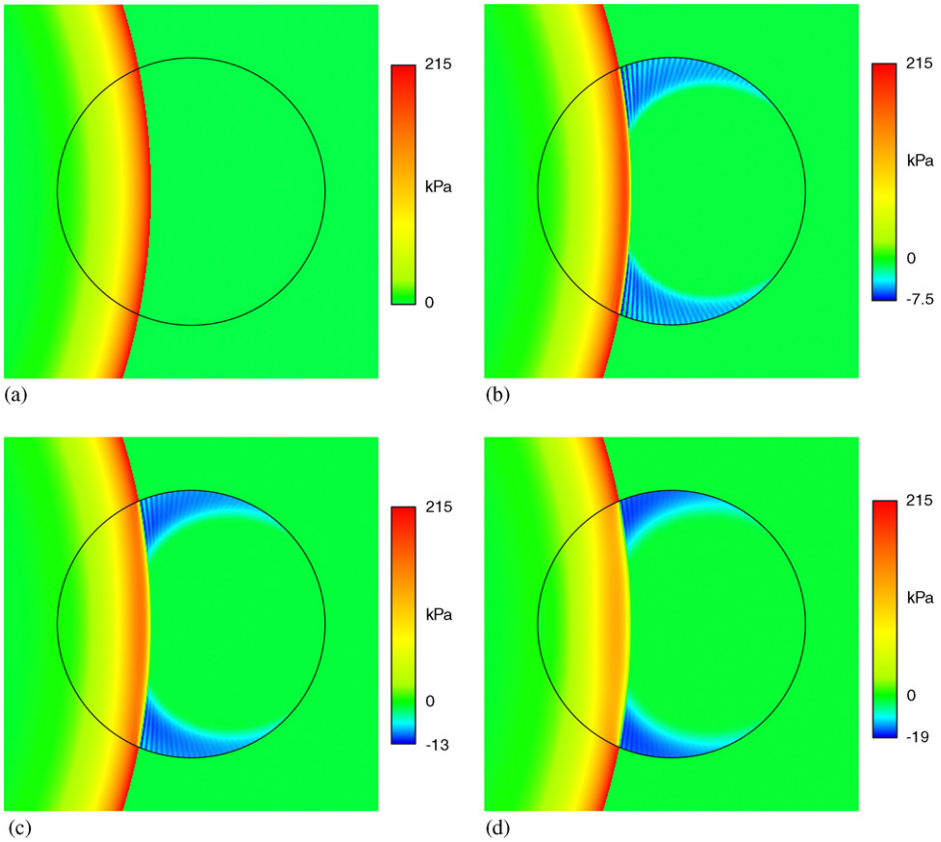

Fig. 8. Acoustic field in a steel shell at $t = 0.70$; (a) in the absence of the shell, (b) $h_0/r_0 = 0.005$, (c) $h_0/r_0 = 0.010$, and (d) $h_0/r_0 = 0.020$.

Next, we compare four shells with the same thickness-to-radius ratio of 0.01 but made of different materials, namely steel with the parameters given above, aluminium ($\rho_a = 2713\,\mathrm{kg/m^3}$, $v_a = 0.334$, and $c_a = 5429\,\mathrm{m/s}$), titanium ($\rho_t = 4509\,\mathrm{kg/m^3}$, $v_t = 0.330$, and $c_t = 4140\,\mathrm{m/s}$), and copper ($\rho_c = 8903\,\mathrm{kg/m^3}$, $v_c = 0.326$, and $c_c = 3868\,\mathrm{m/s}$). Fig. 9 shows acoustic fields inside these shells at $t = 0.70$. One can see that of the three parameters of a shell, i.e. the sound speed, Poisson's ratio, and density, the latter seems to have the most profound effect on the shock transparency. Namely, the higher the density the less transparent the shell is. It is interesting to point out that, even though the circumferential advancements of the internal shock wave are the same for all four systems, those of the shell-induced waves are not which is due to different wave speeds in the materials considered. The difference between the shell-induced fields in the copper and aluminium shells is particularly striking. It is also clear now just how suitable the term 'head waves' is in reference to the shell-induced waves.

For practical purposes, however, it would be beneficial to introduce a parameter that would account for the observed changes of the shock transparency due to varying parameters of the shell. It appears that the dimensionless mass per unit area of the shell,

$$\delta = \frac{h_0}{r_0}\frac{\rho_s}{\rho_f}, \tag{12}$$

can be used for such assessment of the shock transparency. Namely, the smaller δ the more 'shock transparent' a shell is.

The fact that the sound speed in the shell has a limited influence on the shock transparency is not surprising. The sound speed governs the propagation of elastic waves in the shell, and we have shown (Iakovlev, 2006) that the influence of those on the pressure is of second order of magnitude. Furthermore, it can be shown that in the beginning of the interaction Eq. (3) is dominated by two terms, the acceleration one $\partial^2 w^*/\partial\tau^2$ and the pressure term p_s. If we ignore all other terms, the multiplier $1/c_s^2$ will cancel out, and the simplified equation will only depend on one parameter which is exactly δ. Thus, along with the physical considerations, it can also be demonstrated mathematically that the sound speed and Poisson's ratio have little effect on the shock transparency of a shell.

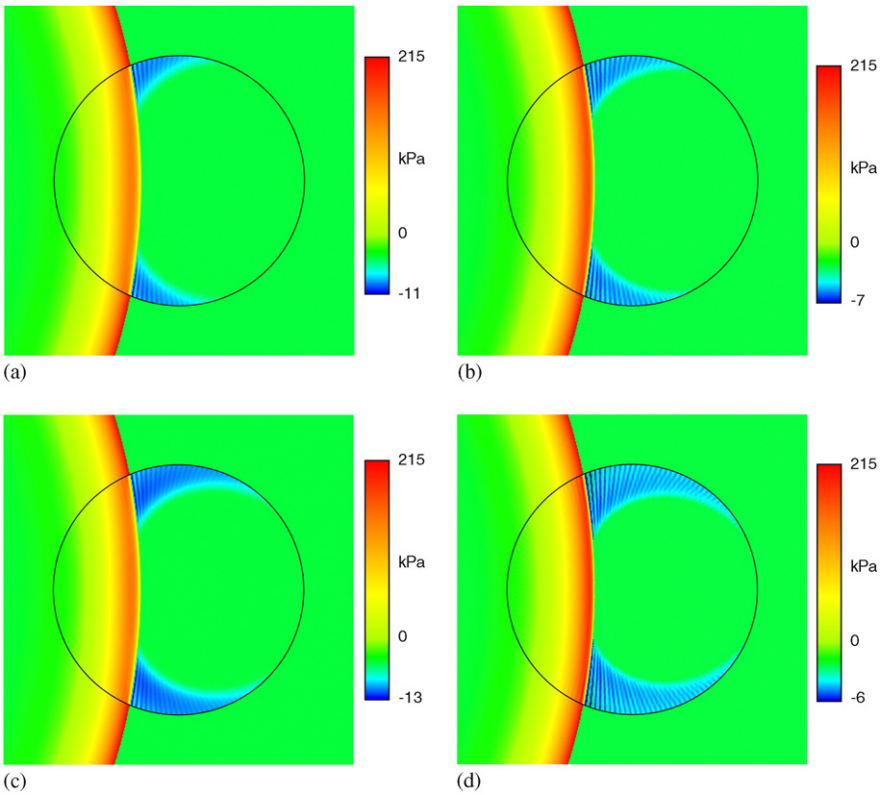

Fig. 9. Acoustic field in a shell with $h_0/r_0 = 0.01$ at $t = 0.70$: (a) copper shell, (b) titanium shell, (c) steel shell, and (d) aluminium shell.

As to the difference between the geometrical and physical parameters of the incident shock wave in the absence of the shell and those of the internal shock wave, it is apparent that the geometry of the 'front' of the internal shock wave is the same as that of the incident wave. Also, it can be shown that the pressure decay behind the 'front' is almost exactly the same as that in the incident shock wave, i.e. the entire process seems to have the same exponential decay rate. In other words, it appears that for a thin shell, the internal shock wave is a geometrical and physical 'continuation' of the incident wave inside the shell. It is important to emphasize that this is true *only if the internal and external fluids are identical*. If the fluids are different, the physics of the interaction is much more complex, and the geometry of the internal shock wave differs from that of the incident one.

Analyzing shock transparency, it is important to remember that the maximum pressure during focusing depends not on the peak incident pressure, but on the peak pressure in the internal shock wave in the beginning of the interaction. The latter depends on the parameters of the shell, and so does the maximum focusing pressure. For example, for the three considered thickness-to-radius ratios of 0.005, 0.01 and 0.02, the maximum focusing pressure exceeds the peak incident one by about 50%, 30%, and 6%, respectively. This reiterates the practical importance of considering all acoustic phenomena in the internal fluid.

7. Fluid–structure interaction on the interface

Throughout the paper, as well as in Iakovlev (2006), we discuss various types of waves propagating in the shell and fluid. To that end, the two-dimensional density plots in polar coordinates we used to display acoustic fields have been very useful, as have been the snapshots of the cross-section of the shell. However, often one's objective is to analyse the pressure dynamics exclusively on the shell surface (this would be the case when, for example, the stress–strain state of a shell is a primary concern). In such a case, it appears that two-dimensional plots of pressure time-history in the t–θ coordinates, i.e. time-space 'unwraps' of the pressure distribution along the shell's circumference, are most suitable. Such a visualization technique is not conventional but is very representative of all aspects of the interaction [e.g., Latard et al. (1999) successfully used the time–space approach in spherical coordinates to analyse wave patterns produced by an elastic spherical structure interacting with an acoustical pulse].

A very useful feature of the t–θ coordinate system is that any wave propagating in the shell with a constant velocity will appear as a straight line with the slope being numerically equal to the dimensionless velocity of propagation. This property is particularly useful as to distinguish shell-radiated waves from all other acoustic effects. We also mention that the bottom of the plot corresponds to the head point and the top to the tail point. This makes t–θ plots especially convenient for analysis of wave reflection and/or superposition at those points.

Fig. 10(a) shows such a t–θ plot of the pressure on the inner surface of the shell, and Fig. 10(b) displays a low-magnitude 'close up' of the pressure field. Two types of waves are seen in the plots. The waves of the first type appear as curves (associated pressures are both high- and low-magnitude), and the waves of the second type are represented by straight lines (low-magnitude pressures only). Note that the plots discussed in this section are particularly informative when analysed along with the sequential snapshots of the internal acoustic field, Fig. 2.

We begin with the analysis of the waves of the first type, and consider the high-magnitude wave represented by the curve W1 starting at the point $(0, 0)$ and terminating at the point $(2, \pi)$. This wave is induced directly by the internal shock wave as it propagates through the fluid and interacts with the shell surface. The wave's velocity of propagation is not a constant relative to the shell, so it appears as a curve. It reaches the tail point at $t = 2$ and no reflected wave of the same order of magnitude is observed on the shell surface, only a small-magnitude reflected wave R2 (marked on the low-magnitude close-up, Fig. 10(b)). This happens because, as we have seen, the high pressures associated with the primary reflection manifest themselves on the shell surface with a considerable delay. This, in particular, prompts us to emphasize that analysing the surface pressure, one should be aware of the fact that often phenomena occurring inside the fluid have no or little *immediate* effect on the surface pressure patterns, and the surface pressure distribution at any particular instant not necessarily reflects the entire acoustic field. We also note that now it is particularly apparent that the highest internal pressure is attained in the shadow zone ($|\theta| > \pi/2$) at times larger than 1, i.e. when the incident wave moved more than half way over the shell, and when the pressure in it decreased quite significantly from what it was in the beginning of the interaction. This is yet another occasion to emphasize the importance of wave phenomena in the system.

At $t \approx 1.4$, a lower-magnitude wave W2 is seen to branch from the 'primary' wave W1. This separation corresponds to transition from Mach to regular reflection, and so the wave W2 represents the Mach stem (the actual transition occurs earlier but is hard to detect in the plots shown). The wave W2 reaches the tail point at $t \approx 2.6$, which corresponds to the collision of the portions of the Mach stems that are in contact with the shell. From then on, the 'primary' reflected wave R1 manifests itself on the shell surface.

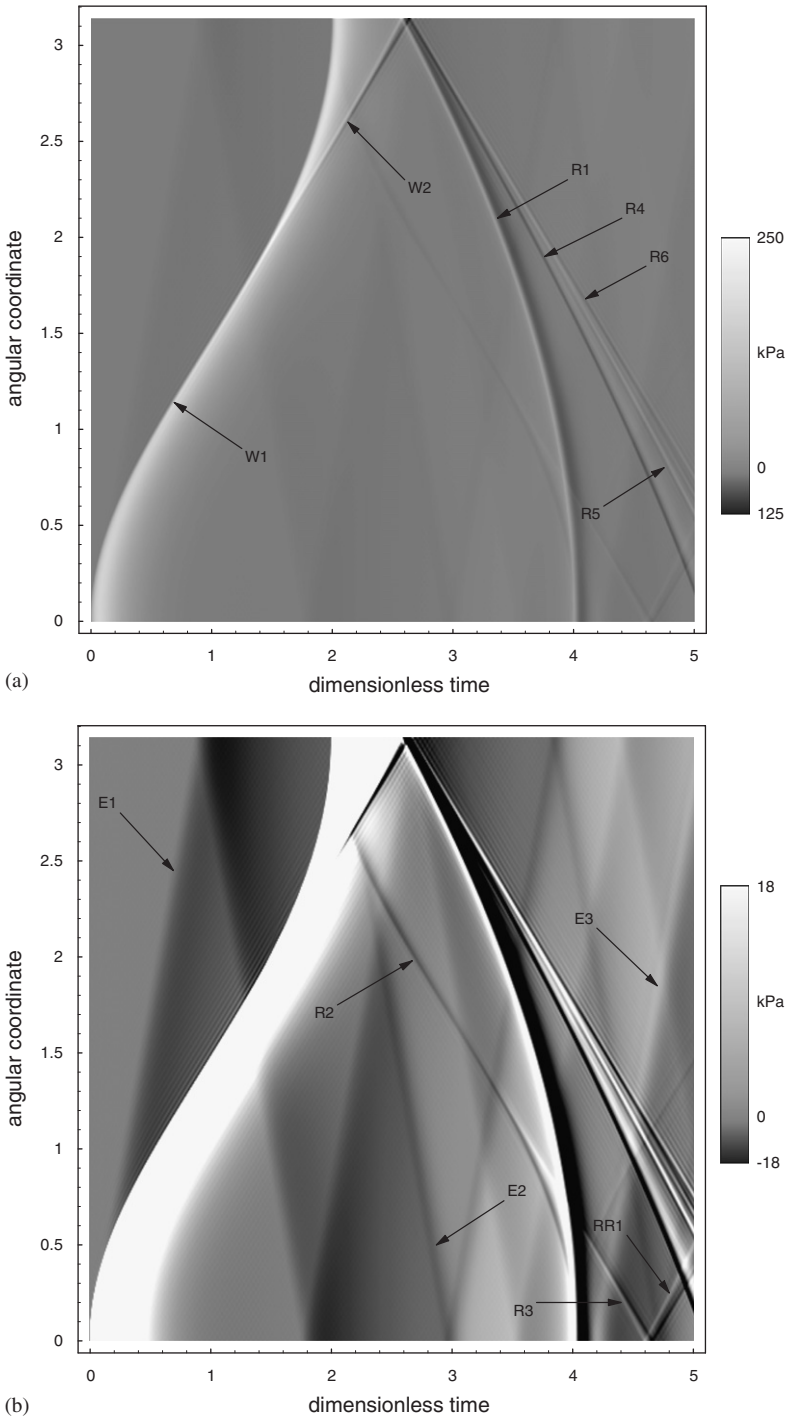

Fig. 10. Pressure on the inner surface of the submerged fluid-filled shell in the t–θ coordinates, $0 \leqslant t \leqslant 5$ and $0 \leqslant \theta \leqslant \pi$: (a) the entire pressure range, and (b) low-magnitude 'close-up'.

The low-magnitude wave R2 originated at the tail point at $t = 2$ corresponds to the 'secondary' reflected wave (Iakovlev, 2006). The pressure in it remains negative throughout the interactions, and its reflection pattern at the head point at $t \approx 3.4-5.0$, Fig. 10(b), is closely resembling that of the wave W1 at the tail point at $t \approx 1.4-3.0$. In particular,

one can observe branching of the wave R3 at $t \approx 3.4$, as well as the series of 'tertiary' reflected waves RR1 which are of the same nature as the wave R1 and the waves R4–R6 which will be discussed shortly.

The slope of the curve corresponding to the primary reflected wave R1 is constantly increasing, and by the time it reaches the head point it appears almost as a vertical line. This is due to the fact that the curvature of the 'front' of this wave is very close to that of the shell surface. A series of low-amplitude reflected waves accompany the wave R1, and one can clearly identify at least three of them, R4, R5 and R6. All of them represent self-similar multiple regular reflections that develop during the late interaction (Fig. 2 and particularly, Figs. 11 and 12 of Iakovlev (2006)). The fact that the waves R4–R6 appear almost as straight lines is purely due to the geometry of the multiple reflected 'wavefronts'. Reflection of these waves from the head region occurs at $t > 5$ and is not considered here. As it was the case with the wave W1, the wave R1 terminates at the head point with no corresponding reflected wave of similar magnitude. Note that even though R1 and R2 have very different geometries, they reach the head point at the exactly same time. Also note that the collision of the Mach stems corresponding to the wave R1 occurs at the head point at $t > 5$, and is not addressed here either.

Now we turn to the low-magnitude waves that appear as straight lines, Fig. 10(b). As we pointed out before, such appearance indicates that the waves in question represent radiation into the fluid of the elastic waves propagating in the shell. As one can see, the overall dynamics of these shell-induced waves is much less complex than that of the acoustic waves. Three distinct waves can be identified in the plot. The first wave, E1, represents radiation by the elastic wave originated in the very beginning of the interaction when the incident shock wave first impinges on the shell. The associated pressure is negative. The second wave, E2, corresponds to the elastic wave originated at the tail point at $t \approx 2$ when the internal shock wave reflects from the tail region. The associated pressure is positive. The third wave, E3, represents the elastic wave originated at $t \approx 4$ at the head point as a result of the secondary reflection of the internal shock wave. The corresponding pressure is negative.

The discussion of the surface pressure would not be complete without comparison of the present case to that of a submerged empty shell. Fig. 11 shows the t–θ plot of the pressure on the outer surface of a submerged evacuated shell subjected to the same shock wave. One can see just how much simpler the physics of the interaction is when no internal fluid is present. There are no complex reflection phenomena during the downstream propagation, and no reflected acoustic waves travelling up- and downstream. The entire interaction is driven by the external acoustic effects, and there is only one shell-induced wave, as opposed to three in the fluid-filled case. It is of particular practical interest that, unlike in the case of a fluid-filled shell, the highest pressure is attained in the head region at the very beginning of the interaction.

Finally, we look at the t–θ plots of the strains in the middle surfaces of the fluid-filled and empty shells, Fig. 12. The difference between the two cases is striking, and one has yet another perspective on the complexity brought into the interaction by the internal fluid. We also mention that, as we have previously seen for a fluid-filled shell (Fig. 3), in the beginning of the interaction there is no significant strain due to the interaction of the internal acoustic wave with the shell, only the strain wave induced by the incident shock when it first impinges on the shell. This phenomenon is particularly clearly illustrated now. One can observe that the first noticeable strain due to the acoustic interaction between the internal shock wave and the shell is observed at $t > 1.8$, i.e. when the wave approaches the tail region. Later ($t \approx 2$), high-magnitude positive strains are induced at the tail point during the primary reflection, and a lower-magnitude wave of negative strains detected at $t > 3.8$ is due to the secondary reflection. In contrast, only one wave of negative strain is travelling around a submerged empty shell.

8. Analysis of the contribution of bending terms

We mentioned earlier (Iakovlev, 2006) that for very thin shells ($h_0/r_0 \leqslant 0.01$) the contribution of the terms representing bending stiffness in the shell equations (2) and (3) (the terms multiplied by k_0^2; for brevity, we refer to them as the 'bending terms') is not significant. In this work, we present the results that led us to that conclusion. Specifically, we simulate the pressure on the inner surface of several different shells using two different models, the complete one that takes all the bending terms into account (i.e. the model with bending stiffness), and the membrane model in which all the bending terms are neglected (and so is bending stiffness), and compare the results. We start with the analysis of the steel shell with $h_0/r_0 = 0.01$.

Fig. 13 shows the surface pressure produced by the two models. The pressure patterns appear to be very similar, and the difference due to the bending terms is difficult to analyse. To make our task easier, we plot the difference separately, Fig. 14(a). Fig. 14(b) depicts a much narrower pressure range.

As one can see, the contribution of the bending terms in this case is limited to a series of extremely high-frequency, low magnitude 'waves'. Even though the maximum magnitude of the contribution of the bending

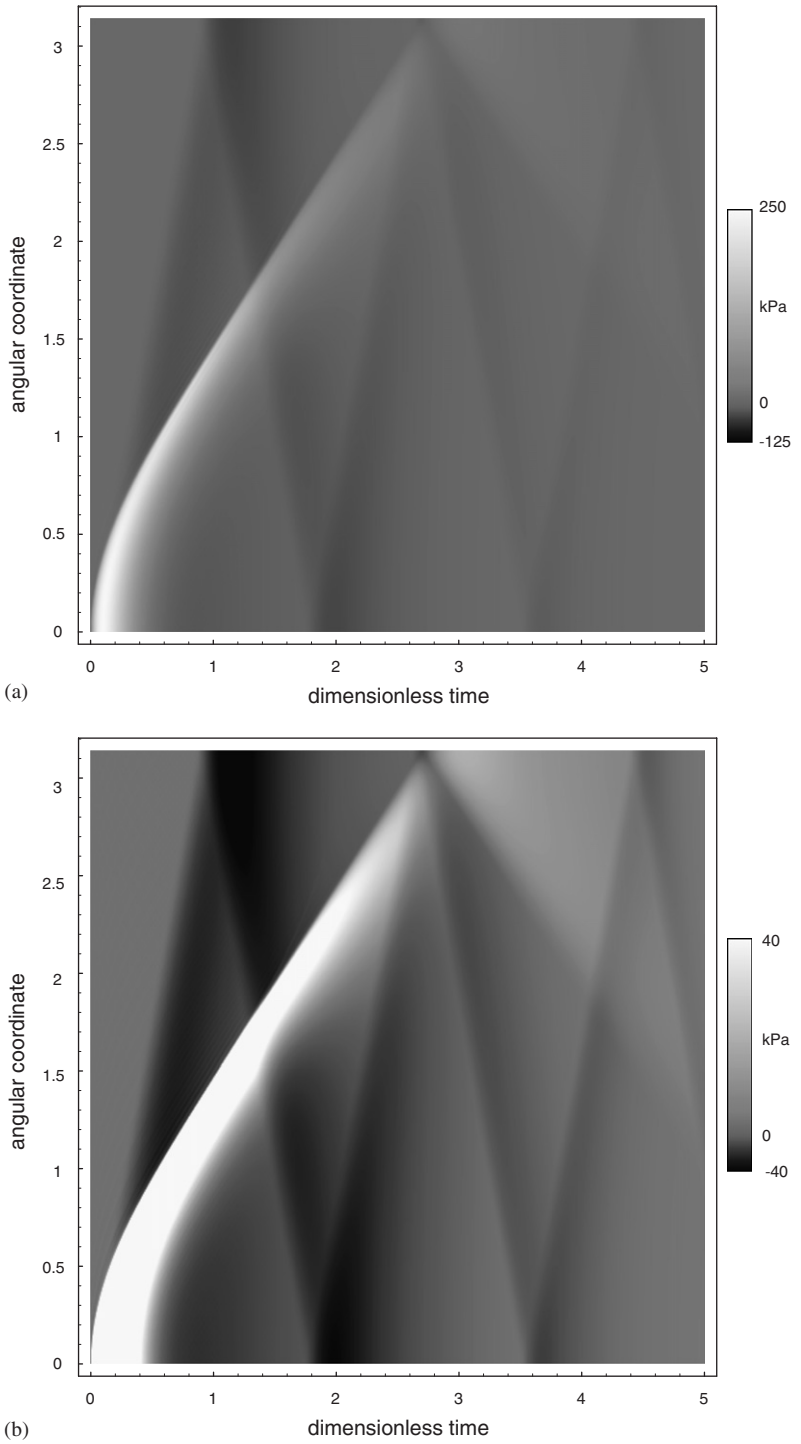

Fig. 11. Pressure on the outer surface of the submerged empty shell in the t–θ coordinates, $0 \leqslant t \leqslant 5$ and $0 \leqslant \theta \leqslant \pi$: (a) the entire pressure range, and (b) low-magnitude 'close-up'.

terms is about 30% of that of the incident pressure, the regions where the maximum values are attained are very localized in space and time. It is also apparent from Fig. 14(b) that one has to consider very low-magnitude pressures (about 1% of the peak incident one) to notice more or less extensive regions

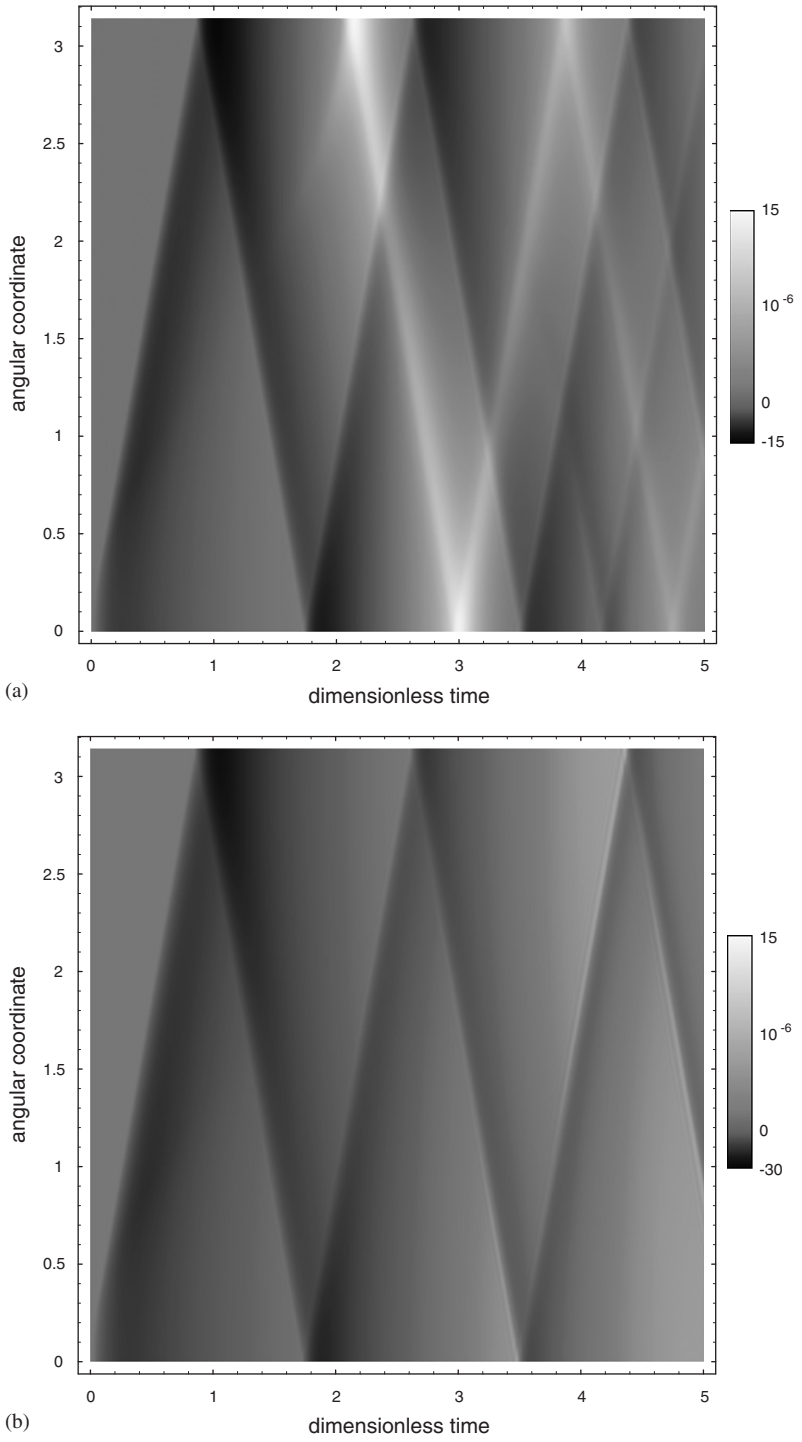

Fig. 12. Strains in the middle surface of the fluid-filled (a) and empty, (b) submerged shells in the t–θ coordinates, $0 \leqslant t \leqslant 5$ and $0 \leqslant \theta \leqslant \pi$.

of the t–θ space affected by the bending terms. Thus, it appears that for a shell with $h_0/r_0 = 0.01$ neglecting the bending terms does not have any significant effect on the distribution of the pressure inside the shell.

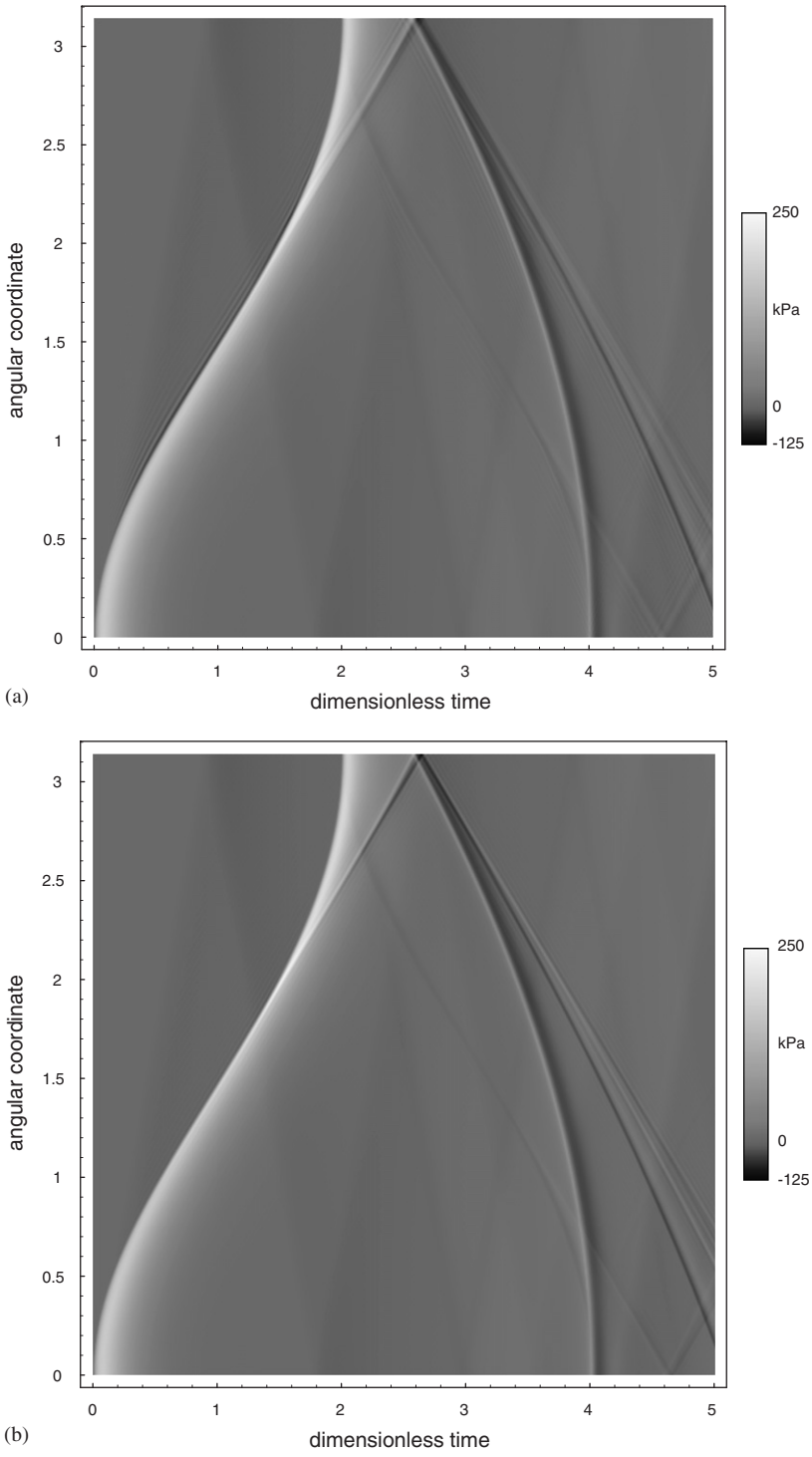

Fig. 13. Pressure on the inner surface of the shell in the t–θ coordinates, $0 \leqslant t \leqslant 5$ and $0 \leqslant \theta \leqslant \pi$; $h_0/r_0 = 0.01$; (a) bending terms are taken into account, and (b) bending terms are neglected.

What happens when the thickness-to-radius ratio is different from 0.01? To answer this question, we consider two more shells, one with the thickness-to-radius ratio of 0.005 and the other with that of 0.02.

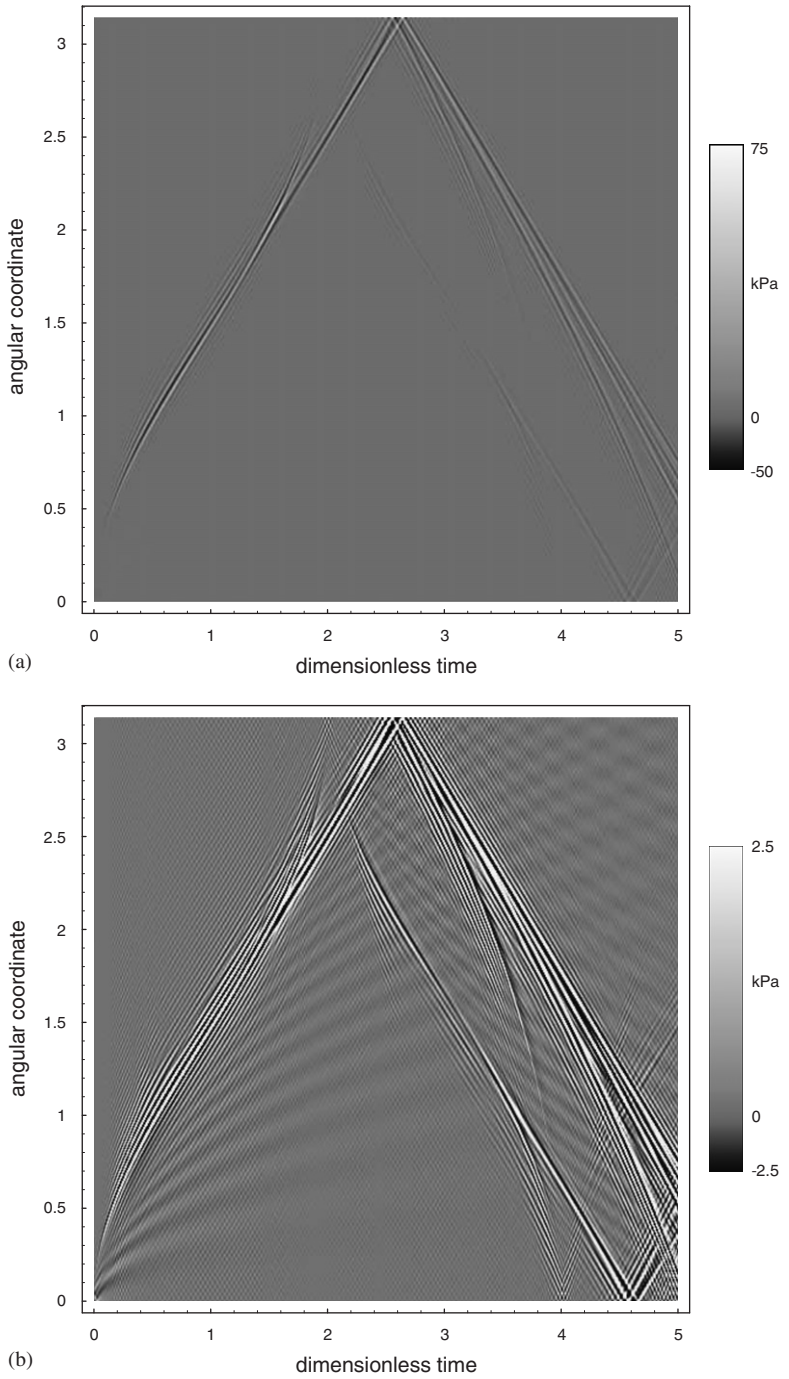

Fig. 14. Difference between the surface pressures produced by the models with and without bending stiffness, $h_0/r_0 = 0.01$: (a) entire pressure range, and (b) low-magnitude close-up.

Fig. 15 shows the difference between the pressures produced by the two models for the thinner shell, $h_0/r_0 = 0.005$ (the pressure patterns themselves are very similar in this case and are not shown). As one can see, the maximum magnitude of the contribution of the bending terms does not exceed 10% of the maximum incident pressure. Furthermore, the frequency of the oscillations contributed by the bending terms is even higher than in the case of

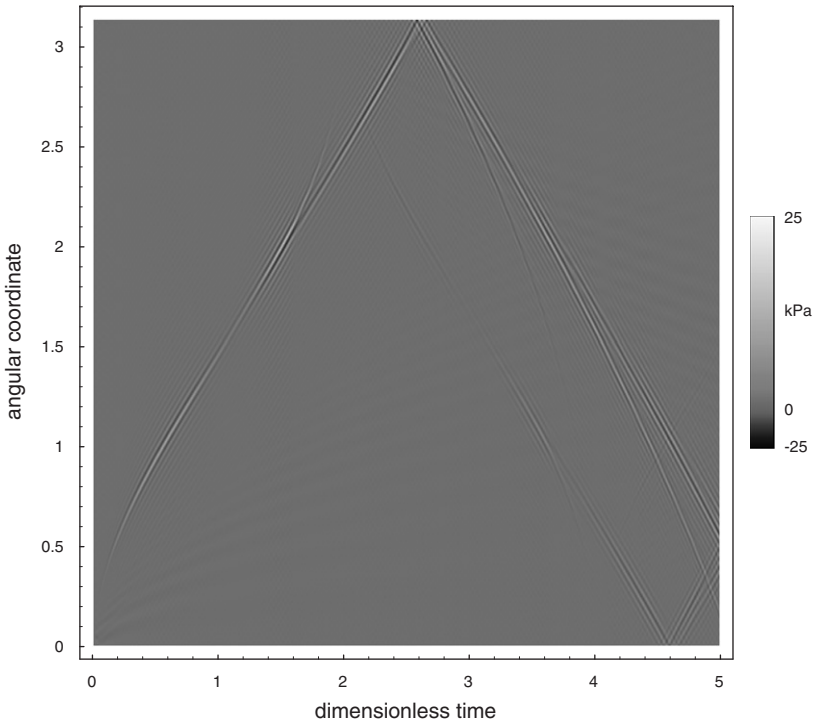

Fig. 15. Difference between the surface pressures produced by the models with and without bending stiffness, $h_0/r_0 = 0.005$.

$h_0/r_0 = 0.01$. Thus, not only the contribution of the bending terms is much lower in magnitude, it is also more localized than in the 'default' case of $h_0/r_0 = 0.01$. So, the bending terms can be neglected for such a thin shell as well.

Finally, Fig. 16 shows the results produced by the two models for the thicker shell, $h_0/r_0 = 0.02$, and the corresponding pressure difference is shown in Fig. 17. One can see that in this case, the magnitude of the contribution of the bending terms is significantly higher (more than 60% of the maximum incident pressure). The frequency of the corresponding pressure oscillations is noticeably lower than in the previous two cases, and the contribution of the bending terms is not localized as much as it was before. Moreover, a pressure close-up at approximately 5% of the maximum incident pressure, Fig. 17(b), reveals extensive regions affected by the bending terms. Thus, even though the acoustic fields produced by the two models are still qualitatively similar, the higher-order effects brought in by the bending terms start to play a much more important role. One therefore has to be careful when applying the membrane model to shells with $h_0/r_0 \geqslant 0.02$, especially if the detailed analysis of the internal pressure field has to be carried out.

In summary, it appears that for thin shells ($h_0/r_0 \leqslant 0.01$) neglecting the bending terms in the shell equations does not lead to any significant changes in the internal acoustic field. For thicker shells, however, careful analysis is needed before the bending terms can be neglected. Even though for such thicker shells the model without bending stiffness is still likely to produce qualitatively acceptable results, the corresponding numerical values could be inaccurate.

9. Cavitation

Finally, one more issue needs to be addressed before the study of the interaction can be considered complete. Namely, we have seen that the pressure in some regions of the internal fluid can be negative. This suggests the possibility of cavitation, since it is known that water, for example, cannot withstand significant tension, and will start to cavitate if pressure falls below a certain critical value (maximum tension water can withstand for very short times is in the 10–100 kPa range [e.g., Makinen (1998)]). Cavitation in the systems of the type considered is a significant engineering concern, and is a challenging phenomenon to study from the researcher's perspective.

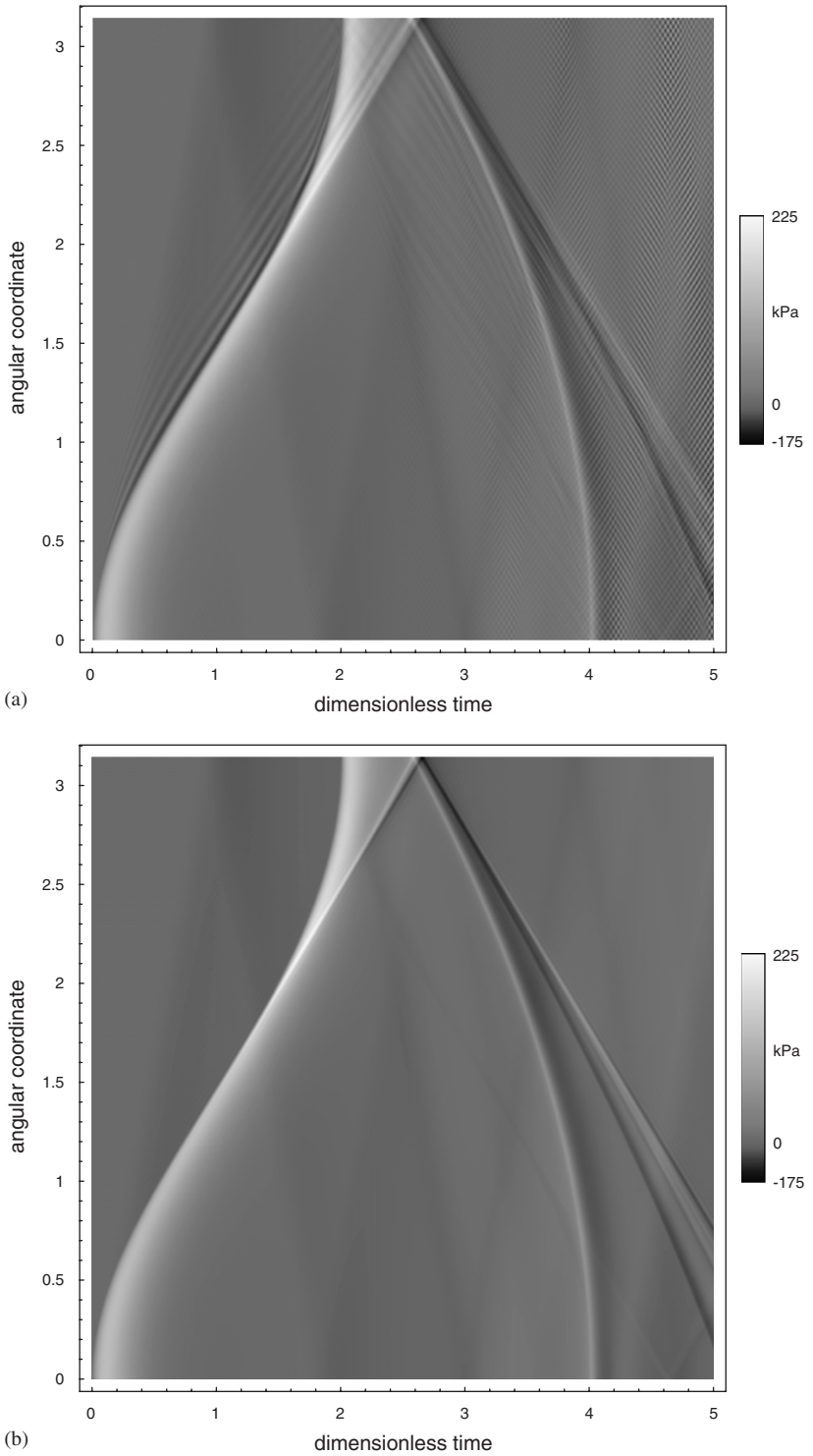

Fig. 16. Pressure on the inner surface of the shell, $h_0/r_0 = 0.02$: (a) bending terms are taken into account, and (b) bending terms are neglected.

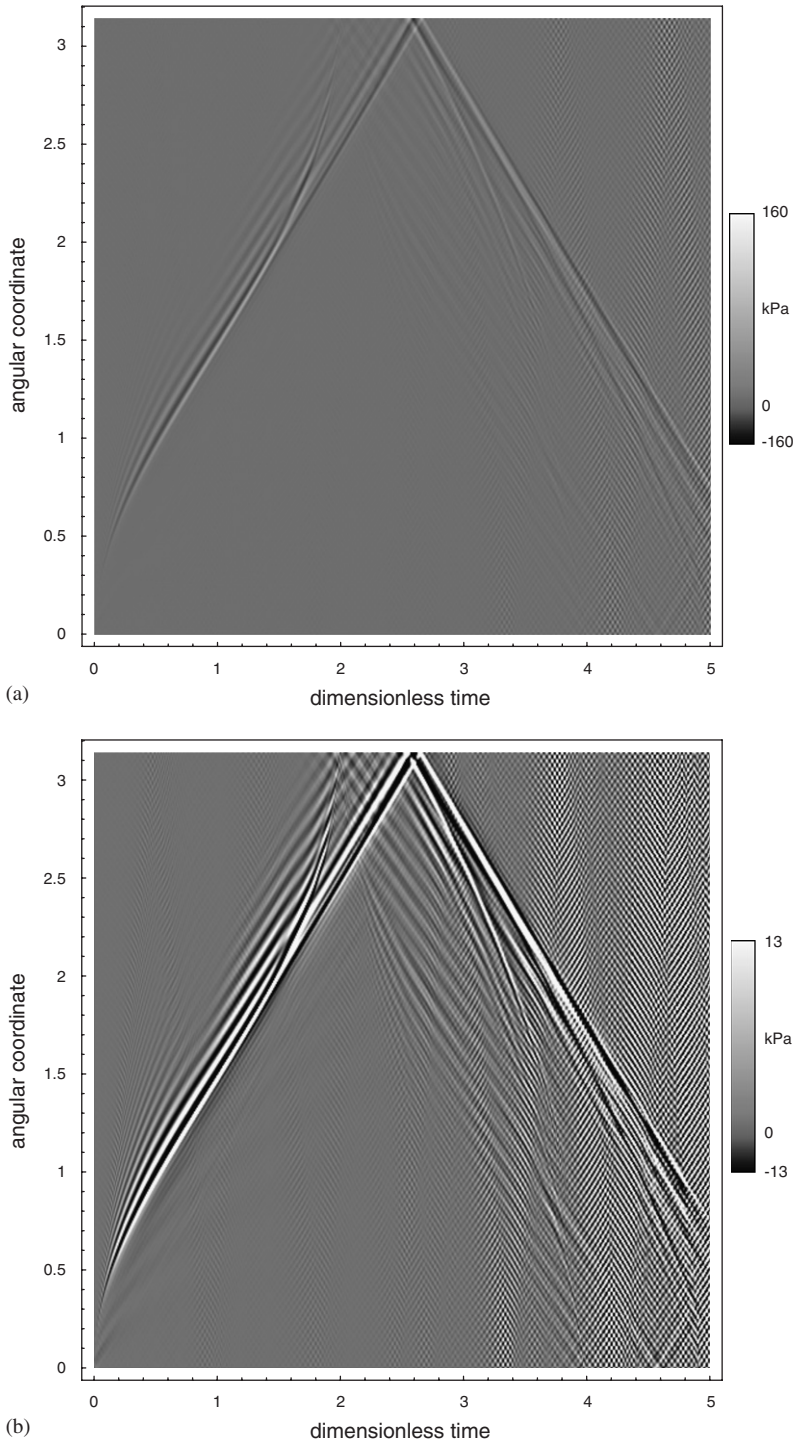

Fig. 17. Difference between the surface pressures produced by the models with and without bending stiffness, $h_0/r_0 = 0.02$: (a) entire pressure range, and (b) low-magnitude close-up.

Cavitation can completely change the dynamics of the interaction. In particular, if it occurs inside the fluid domain (i.e. if the cavitating region does not interact with the shell surface), it usually leads to structure reloading after the cavitation zone collapses [e.g., Wardlaw and Luton (2000)]. If the cavitation region is adjacent to the shell surface,

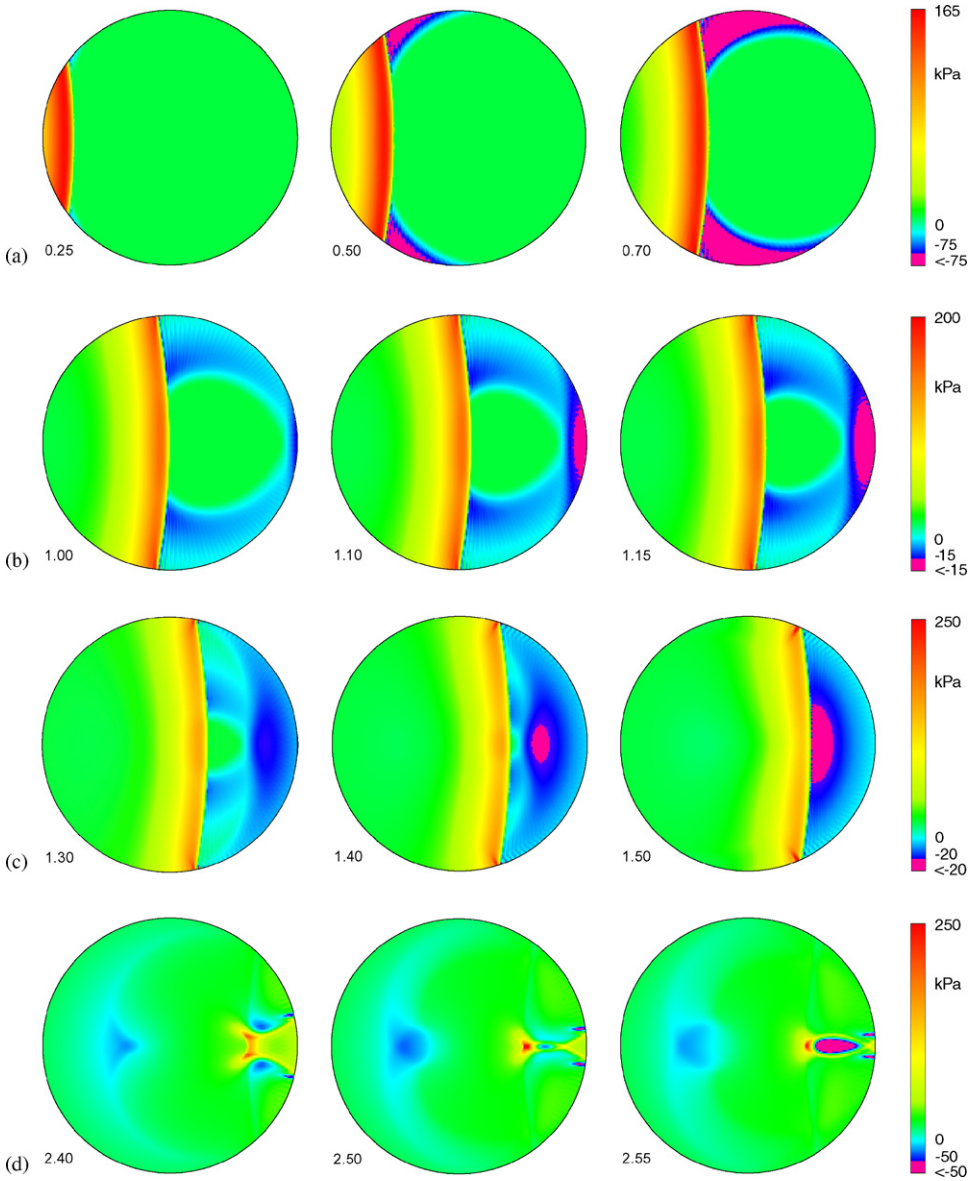

Fig. 18. Cavitation scenarios for four values of the maximum allowable tension in the internal fluid: (a) 7.5 kPa, (b) 15 kPa, (c) 20 kPa and (d) 50 kPa.

separation of the latter from the fluid occurs leading to much higher displacements and deformations [e.g., Makinen (1998)]. When the shell and fluid come in contact again, shell reloading takes place with the pressures comparable to those of the initial shock loading.

Once cavitation occurs, the rest of the interaction is quite different from what is predicted by a model that does not take cavitation into account. Strictly nonlinear phenomena will dominate, and the linear model employed here will be of little use, if any. However, the solution we developed is still useful for predicting the regions where cavitation is likely to develop. Specifically, if we set a certain 'threshold' value of the tension at which the fluid starts to cavitate, it will be easy to visualize the regions prone to cavitation.

We illustrate this idea considering four different values of the maximum tension the fluid is still able to withstand, 7.5, 15, 20, and 50 kPa. Fig. 18 shows pressure patterns before and after the pressure in the fluid falls below the corresponding critical value *for the first time*; magenta colour is used to distinguish the regions where the pressure is lower than the critical value from the rest of the acoustic field.

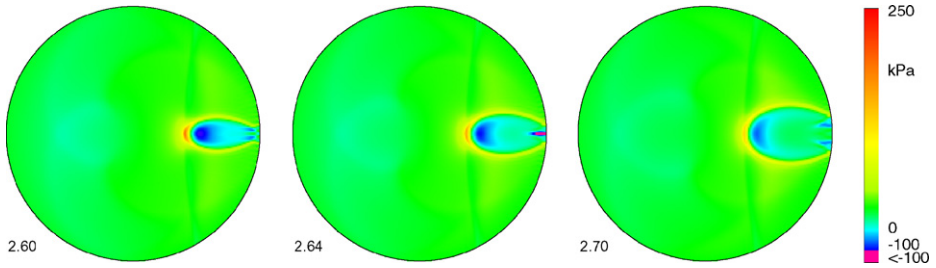

Fig. 19. Regions prone to cavitation during the mid interaction at the maximum allowable tension of 100 kPa.

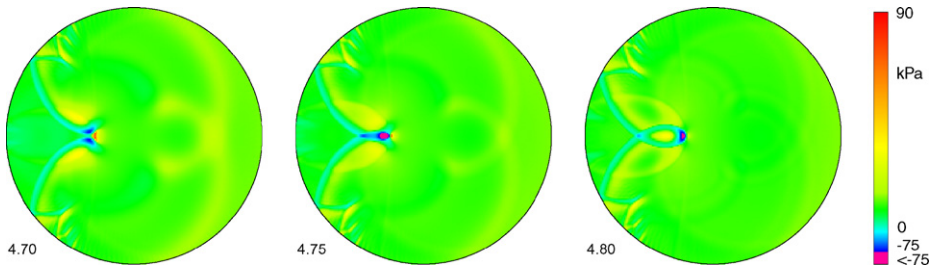

Fig. 20. Regions prone to cavitation during the late interaction at the maximum allowable tension of 75 kPa.

As one can see, different cavitation thresholds lead to completely different cavitation scenarios. For the first threshold, the cavitation starts at the very beginning of the interaction. Massive cavitation zones adjacent to the shell develop, and extensive separation of the shell surface from the fluid is expected to occur. This is probably the worst-case scenario from the modelling point of view since cavitation zones are very extensive and cavitation occurs very early in the interaction. We note that this type of cavitation is entirely due to fluid–structure interaction effects since the internal shock wave has not yet reached the areas affected by cavitation. We also mention that this 'surface' type of cavitation is described in general terms for the case of an external loading in Mair (1999).

For the second threshold, cavitation starts later, at $t \approx 1.00-1.10$, and it develops in the proximity of the tail point. Separation of the shell surface is expected to occur as well, but in this case, because of the already high stresses induced by the superposition of the elastic waves at $t \approx 0.88$, it will likely be more dangerous in terms of the structural response. Note that this cavitation scenario is entirely due to fluid–structure interaction phenomena as well.

In the third case, the scenario is totally different once again, and this time cavitation develops inside the fluid. The cavitation region does not interact with the shell surface, and its eventual collapse will cause reloading of the structure. The fluid–structure interaction nature of cavitation is again the case.

For the fourth maximum allowable tension, cavitation starts within two very local symmetric regions in the close proximity of the shell surface at $t \approx 2.50$, and shortly after that it starts to develop inside the fluid domain as well. From the practical point of view, this scenario is probably the least dangerous since the very local near-wall cavitation regions are not likely to have a significant effect on the dynamics of the shell, and the region inside the fluid is relatively small. Unlike the first three cases, cavitation is now caused exclusively by acoustic phenomena in the internal fluid.

We would like to point out that for the values of the maximum allowable tension in the 10–12 kPa range, cavitation will develop almost simultaneously both on the shell surface and in two symmetric zones inside the fluid. This happens when pressure in the blue zones ahead of the 'wavefront', Fig. 18(b), falls below the critical level. This case is, perhaps, the most complicated in terms of the structural analysis since the shell is likely to experience both the reloading associated with its separation from fluid and that due to collapse of the cavitation zones inside the fluid.

For the maximum allowable tension significantly higher than 50 kPa, cavitation is still possible but it starts during either the mid or late interaction. In particular, we have seen that after the primary and during the secondary focusing pressures as low as -140 and -155 kPa, respectively, are observed. Since the cavitation threshold will almost definitely be above these values, cavitation will develop. From the practical point of view, the possibility of cavitation so late in the interaction means that structure reloading due to cavitation collapse is possible even at times more than twice of what it takes for the incident wave to move over the shell. However, the corresponding regions of low pressure are very

local and exist for a very short time, and so the influence of cavitation on the shell is not expected to be significant. As an example, Fig. 19 illustrates what happens during the mid interaction if the maximum allowable tension is set to 100 kPa, and Fig. 20 shows the regions prone to cavitation during the late interaction at the maximum allowable tension of 75 kPa.

Concluding these remarks about cavitation, we would like to emphasize that even though the influence of the elasticity of the shell on the dynamics of the internal fluid was shown to be of second order of magnitude, it becomes determining when cavitation is a concern. We also emphasize that the discussion presented is mostly hypothesizing based on general understanding of cavitation in the fluid–structure interaction context, and the results presented here should only be viewed as a preliminary theoretical analysis. Numerical simulation using models that take cavitation into account and/or experiments are needed to confidently make any statements about cavitation in shock-interacting shells.

10. Conclusions

We have considered the interaction between a submerged fluid-filled circular cylindrical shell and an external shock wave, and focussed on a variety of fluid–structure interaction phenomena occurring during the interaction. The analysis was based on the semi-analytical solution developed in the author's earlier work (Iakovlev, 2006).

The dynamics of the shell was considered, in particular the strains and normal displacements of the shell surface were analysed. It was found that even though the influence of the elastic effects in the shell on the internal fluid is usually of second order of magnitude, the influence of the acoustic waves in the fluid on the stress–strain state of the shell is much more significant, and the presence of the internal fluid completely changes the dynamics of the interaction.

Special attention was paid to the analysis of the pressure distribution on the shell surface which was performed using two-dimensional time-space plots. It was observed how various waves propagating in the internal fluid manifest themselves on the shell surface, and such images have proven to be a very informative complement to the traditional plots in polar coordinates. Specifically, the acoustic effects associated with shell-induced waves are very easy to distinguish from those related to the internal shock wave using the time-space visualization technique.

The ability of the shell to reduce the intensity of the incident shock as it penetrates the structure, or its 'shock transparency' as we termed it, was investigated as well. Various materials and shell thicknesses were considered, and the effect that they had on the shock transparency of the shell and the geometry of the internal pressure field was analysed. The dimensionless mass per unit area of the shell was proposed as a measure of its 'shock transparency'. It was observed that if the internal and external fluids are identical, the shell does not change the geometry of the incident wave or its decay constant, i.e. the internal pressure wave is a geometrical and physical 'continuation' of the incident wave inside the shell.

The possibility of cavitation in the internal fluid was discussed as well. Such analysis was prompted by the fact that relatively high-magnitude tension was observed to occur in the fluid during the interaction. It was found that different values of the maximum allowable tension correspond to completely different cavitation scenarios. A number of those were discussed using colour images of the internal pressure field. Some of the scenarios considered appeared to be relatively harmless in terms of the structural safety, whereas some seemed to present a serious threat to the structure due to such effects as separation of the shell from the fluid and cavitation zone collapse.

The contribution of the terms representing bending stiffness in the shell equations to the stress–strain state of the shell was analysed as well, and two different models, with and without bending stiffness, were considered. It was found that for shells with the thickness-to-radius ratio of or less than 0.01 ignoring bending stiffness does not result in any qualitatively significant changes in the internal acoustic field. For thicker shells, however, careful analysis is needed since ignoring bending stiffness may lead to considerably incorrect magnitudes of the internal radiation pressure.

The present work completes the study initiated in the companion paper (Iakovlev, 2006). The two papers complement each other and cover a broad spectrum of phenomena, both acoustical and structural, that occur during the shell–shock interaction. The model developed and validated in the papers appears to be suitable for use as a benchmark. It also appears that the approach employed here can be successfully used to study more complex shell systems, in particular those for which experimental data are not yet available.

Acknowledgements

The author gratefully acknowledges the financial support of the Natural Sciences and Engineering Research Council (NSERC) of Canada (Discovery Grant 261949), the Killam Trusts at Dalhousie University, and the Faculty of

Engineering, Dalhousie University. The assistance of Mr Mathew P. Bligh, a Mechanical Engineering student at Dalhousie University, is appreciated as well.

References

Ahyi, A.C., Pernod, P., Gatti, O., Latard, V., Merlen, A., Uberall, H., 1998. Experimental demonstration of the pseudo-Rayleigh (A_0) wave. Journal of the Acoustical Society of America 104, 2727–2732.

Andelfinger, U., 1994. Simulations of underwater explosions against submerged structures using the DYSMAS/ELC code—Part A. Proceedings of the 65th Shock and Vibration Symposium, vol. II, San Diego, CA, USA, pp. 243–251.

Bryson, A.E., Gross, R.W.F., 1961. Diffraction of strong shocks by cones, cylinders, and spheres. Journal of Fluid Mechanics 10, 1–16.

Geers, T.L., 1969. Excitation of an elastic cylindrical shell by a transient acoustic wave. Journal of Applied Mechanics 36, 459–469.

Heilig, G., 1999. Shock-induced flow past cylinders with various radii. Proceedings of the 22nd International Symposium on Shock Waves, Imperial College, London, UK, pp. 1099–1104.

Heilig, W.H., 1969. Diffraction of a shock wave by a cylinder. Physics of Fluids 12 (Supplement I), 154–157.

Hermann, D., Weblau, F.P., Adomeit, G., 1987. Measurements of heat transfer and vortex shedding frequency of cylinders in shock tube cross flow. In: Proceedings of the 16th International Symposium on Shock Tubes and Waves, Aachen, Germany, pp. 822–830.

Huang, H., 1979a. Transient response of two fluid-coupled spherical elastic shells to an incident pressure pulse. Journal of the Acoustical Society of America 65, 881–887.

Huang, H., 1979b. Transient response of two fluid-coupled cylindrical elastic shells to an incident pressure pulse. Journal of Applied Mechanics 46, 513–518.

Huang, H., Wang, Y.F., 1970. Transient interaction of spherical acoustic waves and a cylindrical elastic shell. Journal of the Acoustical Society of America 48, 228–235.

Iakovlev, S., 2002. Interaction of a spherical shock wave and a submerged fluid-filled circular cylindrical shell. Journal of Sound and Vibration 225, 615–633.

Iakovlev, S., 2006. External shock loading on a submerged fluid-filled cylindrical shell. Journal of Fluids and Structures 22, 997–1028.

Junger, M.C., Feit, D., 1972. Sound, Structures, and their Interaction. MIT Press, Cambridge, USA.

Latard, V., Merlen, A., Preobazhenski, V., Ahyi, A.C., 1999. Acoustic scattering of impulsive geometrical waves by a glass sphere in water. Applied Physics Letters 74, 1919–1921.

Mair, H.U., 1999. Review: hydrocodes for structural response to underwater explosions. Shock and Vibration 6, 81–96.

Makinen, K., 1998. Cavitation models for structures excited by a plane shock wave. Journal of Fluids and Structures 12, 85–101.

Merlen, A., Pernod, P., Ahyi, A., Kemmou, A., 1995. Shock-wave diffraction by an elastic sphere in water. Proceedings of the 20th International Symposium on Shock Waves, vol. I, Pasadena, CA, USA, pp. 513–518.

Mindlin, R.D., Bleich, H.H., 1953. Response of an elastic cylindrical shell to a transverse step shock wave. Journal of Applied Mechanics 20, 189–195.

Oakley, J.G., Anderson, M.H., Wang, S., Bonazza, R., 2001. Shock loading of a cylinder bank with imaging and pressure measurements. Proceedings of the 23rd International Symposium on Shock Waves, Fort Worth, Texas, USA, pp. 589–595.

Ofengeim, D.Kh., Drikakis, D., 1997. Simulation of blast wave propagation over a cylinder. Shock Waves 7, 305–317.

Sun, M., Yada, K., Jagadeesh, G., Odonera, O., Ogawa, T., Takayama, K., 2003. A study of shock wave interaction with a rotating cylinder. Shock Waves 12, 479–485.

Takano, Y., Hayashi, K., Goto, T., A computational procedure for interactions of shock waves with solid materials in liquid. Proceedings of the 21st International Symposium on Shock Waves, Great Keppel Island, Australia, pp. 1039–1044.

Takayama, K., 1987. Holographic interferometric study of shock wave propagation in two-phase media. In: Proceedings of the 16th International Symposium on Shock Tubes and Waves. Aachen, Germany, pp. 52–62.

Wardlaw Jr., A.B., Luton, J.A., 2000. Fluid–structure interaction mechanisms for close-in explosions. Shock and Vibration 7, 265–275.